DROPLET TRANSPORT IN TURBULENT PIPE FLOW

Theodore Ginsberg

U of C-AUA-USAEC

ARGONNE NATIONAL LABORATORY, ARGONNE, ILLINOIS

Printed in the United States of America
Available from
National Technical Information Service
U.S. Department of Commerce
5285 Port Royal Road
Springfield, Virginia 22151
Price: Printed Copy $3.00; Microfiche $0.95

ANL-7694
Engineering and Equipment

ARGONNE NATIONAL LABORATORY
9700 South Cass Avenue
Argonne, Illinois 60439

DROPLET TRANSPORT IN TURBULENT PIPE FLOW

by

Theodore Ginsberg

Engineering and Technology Division

Based on a thesis submitted to
the Graduate School of
The Pennsylvania State University,
Department of Nuclear Engineering,
in partial fulfillment of the requirements
for the degree of
Doctor of Philosophy

November 1971

TABLE OF CONTENTS

TABLE OF CONTENTS (Contd.)

LIST OF FIGURES

LIST OF TABLES

NOMENCLATURE

In this nomenclature, the symbols used for quantities with dimension are: L for length, T for time, M for mass, θ for temperature, and V for volts. Dimensions are indicated within the brackets following their definition. Dimensionless quantities have no brackets following their definition.

a	droplet radius (L)
c	fluctuating droplet concentration (M/L^3)
C	mean droplet concentration (M/L^3)
$\overline{C}$	mean droplet concentration (M/L^3)
C*	local droplet mass concentration (M/L^3)
C_d	droplet concentration (M/L^3)
CMAX	droplet concentration at r = 0 (M/L^3)
C_w	droplet concentration at wall (M/L^3)
d,d'	droplet diameter (L)
D	duct diameter (L)
D_o	molecular diffusion coefficient for water vapor in air (L^2/T)
D_p	molecular diffusion coefficient for property P (L^2/T)
e	fluctuating anemometer output voltage (V)
e_d	droplet voltage pulse (V)
e_g	fluctuating voltage - air flow only (V)
E	mean anemometer output voltage (V)
E_p	$=\varepsilon_p/V_p$ (L)
g	gravitational acceleration (L/T^2)
G	defined by Equation (3-11)
h_{fg}	heat of vaporization (Btu/M)

I_0 zeroth order Bessel function

$\vec{J}$ vector droplet number flux ($1/L^2T$)

J_z scalar axial droplet number flux ($1/L^2T$)

k mass transfer coefficient (L/T)

L duct length dimension used in L/D ratio

L_E transverse Eulerian integral scale (L)

m droplet mass (M)

$\dot{m}$ droplet mass flux (M/L^2T)

M total mass velocity (M/L^2T)

N droplet number concentration ($1/L^3$)

p, p_i partial pressure of water vapor (M/LT^2)

P arbitrary property

P_o static pressure at 1st pressure port (M/LT^2)

P_s static pressure (M/LT^2)

q_h wall heat flux (Btu/L^2T)

q_p turbulent flux of pr

r,r' radial coordinate (L)

R duct radius (L)

R_L Lagrangian fluid particle correlation function

R_o gas constant ($ML^2/T^2\theta$)

R_{22} transverse Eulerian correlation function

Re Reynolds number = DU_o/ν

S droplet source (sink) rate (M/L^3T)

t,t' time (T)

T particle response time (T)

T_L Lagrangian temporal integral scale (T)

T_o absolute temperature (θ)

u — axial component of turbulent velocity (L/T)

u_i — i th component of Eulerian turbulent fluid velocity (L/T)

u_t — particle terminal velocity (L/T)

u^* — droplet deposition velocity (L/T)

$\vec{u}$ — turbulent velocity vector (L/T)

$\overline{u^2}$ — mean square turbulent velocity (L^2/T^2)

U — local mean air velocity (L/T)

U_o — mean axial air velocity at r = 0 (L/T)

U_r — relative velocity between droplet and air (L/T)

$\vec{U}$ — vector fluid velocity (L/T)

v — radial component of turbulent fluid velocity (L/T)

v_i — i th component of fluctuating particle velocity (L/T)

$\vec{v}$ — local fluctuating vector droplet velocity (L/T)

V — local mean particle velocity (L/T)

V_p — scalar mean axial velocity (L/T)

$\vec{V}$ — local vector droplet velocity (L/T)

$\vec{V}_p$ — local mean vector droplet velocity (L/T)

y — spatial coordinate (L)

$\overline{y^2}$ — mean square molecular displacement (L^2)

z — axial coordinate measured from plane source (L)

z' — axial coordinate measured from point source (L)

Greek terms

δ — Kronecker delta function

ε — turbulent diffusivity for property P (L^2/T)

ε_f — turbulent mass diffusivity (L^2/T)

ε_p — turbulent particle diffusivity (L^2/T)

ε_T	turbulent thermal diffusivity (L^2/T)
μ	air viscosity (M/L-T)
ν	air kinematic viscosity (L^2/T)
ρ_f	fluid density (M/L^3)
ρ_p	particle density (M/L^3)
σ	fluid particle displacement (L)
$\overline{\sigma^2}$	mean square fluid particle displacement (L^2)
σ_p	particle (droplet) displacement (L)
$\overline{\sigma_p^2}$	mean square particle (droplet) displacement (L^2)
τ	time (T)
ϕ_1	defined by Equation (3-8a)
ϕ_2	defined by Equation (3-8b)
∇	gradient operator (1/L)

DROPLET TRANSPORT IN TURBULENT PIPE FLOW

by

Theodore Ginsberg

ABSTRACT

Analytical and experimental investigations of the Fick's law diffusion model of turbulent droplet transport are described here. The turbulent diffusion model is applied to the transport of liquid droplets in the central core region of fully developed turbulent pipe flow.

The Fick's law formulation is defined, and its implications are discussed. The particle diffusivity is defined in terms of the statistical properties of the particulate motion. The momentum equations for a single particle moving in a turbulent fluid are presented. An expression for the particle diffusivity is obtained for the case of a particle falling with terminal velocity greater than the rms turbulent fluid velocity.

A study of droplet transport in turbulent pipe flow was carried out. Water droplets, introduced into the center of a pipe, flowed vertically downward and concurrently with the air flow. A droplet generator was fabricated which produced a continuous stream of uniform size droplets with known diameter. Radial distributions of the droplet concentration were measured downstream from the droplet injector. A hot wire anemometer was employed as a droplet concentration sensor.

The droplet concentration data were used to extract particle diffusivity information. For each droplet size, Reynolds number and axial measurement station, a least squares analysis yielded a value of the diffusivity.

I. INTRODUCTION

An important consideration in the design of liquid-cooled or boiling nuclear reactors is the possible occurrence of a critical convective heat transfer condition. This condition, frequently referred to as boiling burnout, results in a relatively sudden change in convective heat transfer characteristics from "good" to "poor." Both the rapidity of the change and the relative difference between "good" and "poor" heat transfer depend on the particular boiling regime at which the critical condition occurs. These different boiling regimes are characterized mainly by the relative amounts of liquid and vapor present.

The particular regime of interest here is characterized by a highly dispersed flowing mixture of vapor and liquid. The major portion of the duct cross section is occupied by a relatively dilute (large vapor volume fraction) suspension of droplets carried along with the turbulent vapor. This regime is frequently referred to as fog flow.

Models of the critical heat transfer condition in high vapor volume fraction flows have been proposed which incorporate some mathematical description of turbulent droplet transport. It has been postulated that this transport process is responsible for the motion of droplets transverse to the duct axis. This motion leads to droplet deposition at the duct walls and to the removal of energy from the heated walls by evaporation. Droplet deposition, therefore, represents a mechanism of cooling the walls which may prevent or delay the onset of a critical heat transfer condition.

Two distinct mathematical descriptions of turbulent droplet transport may be found in the critical heat transfer literature. Neither of these descriptions has been clearly defined. The conditions under

which one or the other would be more useful in the formulation of a theory of the occurrence of a critical heat transfer condition have not been established.

The purpose of this investigation was to study one of these droplet transport descriptions. The basis of this description is a Fick's law representation for the turbulent flux of droplets. The Fick's law, or turbulent diffusion, model was applied to the description of droplet transport in adiabatic, turbulent pipe flow.

II. LITERATURE REVIEW

The first section of this chapter reviews the literature dealing with the critical heat transfer condition in the convective boiling regimes. Particular emphasis is placed on the fog flow boiling regime and on the proposed models of the droplet transport process which are found in the critical heat transfer literature. The discussion of the turbulent diffusion literature reviews past work on the statistical theory of turbulence and on the eddy diffusion model of turbulent transport. The last section is a discussion of past investigations concerning the transport of particulate matter in turbulent flow.

2.1 The Critical Heat Transfer Condition

2.1.1 Boiling Regimes in Forced Convection Flow

Observation of liquid-gas flow systems has indicated the existence of a continuous range of possible boiling regimes. A brief description of current ideas of different boiling regimes in forced convection flow follows.

The flow of an initially subcooled liquid through a long, heated duct is traced in Figure 1.[1] The fluid leaves the duct as saturated vapor. There is no boiling in Region 1. The bulk liquid in Region 2 is subcooled; bubble generation takes place in a superheated region near the surface. These bubbles condense as they are swept into the subcooled bulk liquid. In Region 3, the bubble flow regime, the bulk liquid is saturated. Bubbles coalesce in the central region of the duct. Region 4, the slug flow regime, is characterized by the presence of large slugs of vapor, occupying nearly the entire duct cross section. The annular flow regime of Region 5 is visualized as one in which liquid flows as a

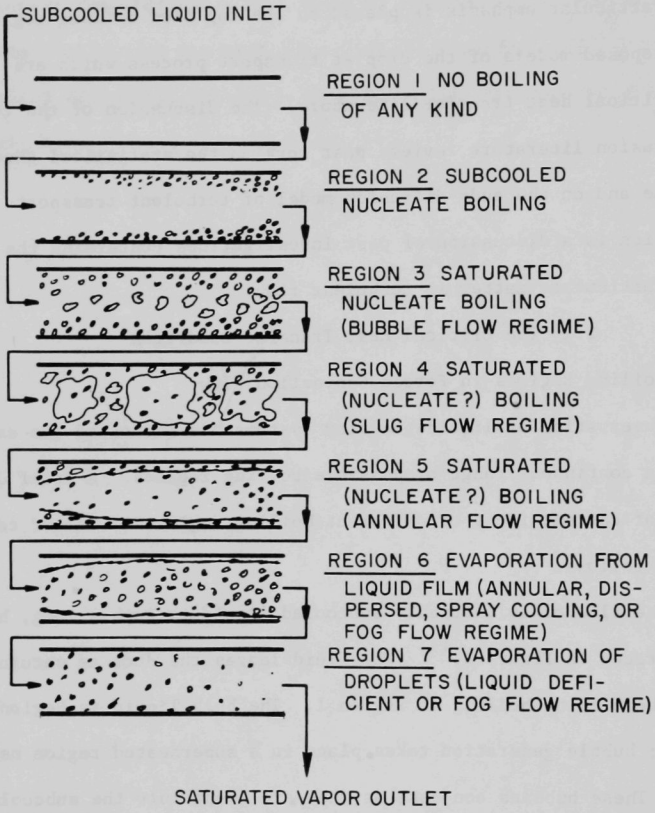

Fig. 1. Vaporization of a Liquid Flowing through a Heated Duct(1)

thin film along the duct walls; most of the vapor is contained in the central core. Vaporization occurs as small bubbles within the liquid film. Liquid is dispersed in the vapor in the form of droplets. Droplet deposition from the turbulent vapor core acts to replenish the liquid film. In Region 6, also termed an annular flow regime (and sometimes called the fog flow regime), vaporization occurs only from the liquid film interface. Region 7, usually referred to as the fog flow regime, is one in which all the liquid is completely dispersed as droplets in the vapor phase. This regime probably occurs only for very high vapor quality flows.

2.1.2 The Fog Flow Regime

There are differences in the literature pertaining to the use of the term fog flow, relating to the presence of a liquid film and its structure. These differences appear to be a result of the lack of distinct boundaries between the different flow regimes described above. The intent here is to define that flow regime which is subsequently denoted as fog flow.

The annular, annular-dispersed, or dispersed regime (Region 6 in Figure 1) has also been called a fog flow regime. These terms have been used to imply a regime in which the liquid phase exists both in the form of droplets dispersed in the vapor and as a thin, flowing liquid film. Two distinct qualitative pictures of the liquid film have been implied by use of the term fog flow. The first, incorporated in the unstable liquid film model,[2,4,5] has implied that liquid is continually ejected from the liquid film in the form of droplets. The process of liquid ejection is called entrainment. The second picture of the film has been considered in the stable liquid film model.[2,3,6,7] In this model, en-

trainment is considered an insignificant mass transfer mechanism. Presumably, there is a region of high vapor volume fraction and high flow rate in which mass transfer by entrainment is negligible and in which the stable film model is applicable.

The term fog flow is reserved for the following two phase regime in forced convection flow: A region of high vapor volume fraction and high mass flow rate in which the bulk of the liquid phase is dispersed as droplets in the turbulent vapor core. If a liquid film exists, then it is assumed stable.

2.1.3 Theories of the Occurrence of a Critical Heat Transfer Condition in High Quality Flow Regimes

Several qualitatively distinct theories of occurrence of a critical heat transfer condition in the annular and fog flow regimes appear in the literature. The essential difference between the theories lies in the relative importance assigned to the mechanisms of entrainment and droplet deposition. Turbulent diffusion of droplets has been considered responsible for droplet deposition.

In developing a theory based on an unstable liquid film model, Hewitt and Lacey[15] assumed that a critical condition occurs when the liquid film is completely torn away from the wall by hydrodynamic forces. The problem of liquid film stability is outside the scope of this work and is not considered further.

Vanderwater,[8] and later Isbin et al.[4] proposed a model based on an unstable film theory. They assumed that entrainment occurs continually, along with droplet deposition on the film and evaporation from the liquid film. According to this theory, if the rate of droplet deposition on the film is insufficient to replace the losses by entrainment

and evaporation, the liquid film thickness reduces to zero and a critical condition occurs.

Grace[5] considered droplet transport from the core to the wall a negligible mechanism for mass transfer. He argued that in most situations of practical interest, there would be a negligible amount of droplets dispersed in the vapor core of the annular flow. According to Grace, therefore, there is no mechanism at play to replenish the losses from the film taking place because of entrainment and evaporation. Grace assumed that a critical condition occurs when the film flow rate diminishes to zero.

Application of the theories discussed above requires no knowledge of the liquid film thickness prior to the onset of a critical heat transfer condition. Tippets[3] attempted to develop a more sophisticated theory which included the effect of liquid film stability. Tippets' work, however, reveals that his mathematical formulation is identical to the formulation based on the stable film model; he finally assumed that entrainment is negligible at the onset of a critical heat transfer condition. Tippets assumed that a critical condition occurs when the film thickness diminishes to zero.

Stein[2] proposed a stable liquid film model of the critical heat transfer condition. He considered a flowing liquid film from which entrainment is negligible. According to this model, liquid is evaporated from the film at the boundary between the film and the vapor core. Stein assumed that a critical condition occurs when the rate of evaporation exceeds the rate of droplet supply to the film.

A further simplication of the stable film model was proposed by Goldmann et al.[6] and was developed further by Stein.[2] They postu-

lated that there exists a flow regime in which the existence of a liquid film can be neglected. Vapor generation occurs as droplets deposit and evaporate on the duct walls. A critical condition occurs, according to this negligible film model,[2] when the rate of droplet deposition is insufficient to remove the energy generated in the wall.

2.1.4 Droplet Transport Representations as Found in the Critical Heat Transfer Literature

Two distinct mathematical formulations for the calculation of deposition rates of droplets on duct walls may be found in the critical heat transfer literature. Both formulations were developed to describe the mechanism of turbulent droplet transport in duct flow.

The mass transfer coefficient formulation assumes that the rate of droplet transport from the turbulent vapor-liquid core to the duct boundary is

$$\dot{m} = k(\overline{C} - C_w), \tag{2-1}$$

where $\overline{C}$ is an average droplet concentration in the core region, C_w is the concentration at the wall, and k is a "film coefficient for mass transfer."[6] The implication of this formulation is that droplets diffuse readily in the core region, but are hindered in their travels by a thin, relatively stagnant, film of vapor near the wall. Application of this formulation requires some assumption relating k to flow parameters. In addition, a boundary condition is required in the form of a restriction on C_w.

Vanderwater[8] and Isbin et al.[4] assumed that $k = bM^j$, where b and j are empirical constants, and M is the total (liquid plus vapor) mass flow rate. In addition, the authors assumed that C_w is zero, since

"the droplets unite with the annular liquid film upon striking it." Goldmann et al.[6] estimated the film coefficient by proposing an analogy between droplet transport and fluid momentum transport. They pointed out, however, that the analogy cannot be expected to be very accurate for droplet transport. The authors assumed that the wall concentration, C_w, is zero since, they stated, the wall is a "droplet sink."

Tippets[3] attempted to construct a more detailed model of the mass transfer and hydrodynamic phenomena taking place prior to the onset of the critical heat transfer condition. Turbulent mixing length arguments were employed in estimating velocity and concentration gradients at the liquid film surface. Tippets' final result, however, is equivalent to that of the mass transfer coefficient approach. In addition, Tippets assumed that the droplet concentration at the liquid film is zero.

Stein[2,9] proposed a second approach to the droplet transport problem. He wrote differential equations of mass balance for the gas and liquid phases. Stein assumed that droplets are carried along with the mean vapor velocity. He applied the following mass conservation equation to the transport of liquid droplets:

$$\vec{U} \cdot \nabla C_d + \nabla \cdot \vec{J} = 0. \qquad (2\text{-}2)$$

The first term represents the convection of liquid with the mean vapor velocity $\vec{U}$. The second term represents the transport of droplets by the turbulent gas. Stein assumed that the turbulent droplet flux, $\vec{J}$, is described by the Fick's law formulation

$$\vec{J} = -\varepsilon_p \nabla C_d, \qquad (2\text{-}3)$$

where ε_p is the turbulent particle diffusivity.

Stein proposed the boundary conditions that apply to Equation (2-2). These characterize the particular fog flow model being considered. For the wall condition applicable to the negligible liquid film model, Stein proposed that the rate of diffusion of droplets to the wall is equal to the rate of evaporation. In the case of pipe flow,

$$\left(-\varepsilon_p \frac{\partial C_d}{\partial r}\right)_{r=R} = q_h/h_{fg}, \tag{2-4}$$

where h_{fg} is the heat of vaporization and q_h is the heat flux at the wall. If q_h is independent of circumferential position then the formulation is a two-dimensional one. Stein assumed that a critical condition occurs when the droplet concentration at the wall is zero. The boundary condition that Stein proposed for application to stable film model is that the rate of diffusion of droplets to the film is equal to the rate of deposition. In mathematical terms, this condition states that

$$\left(-\varepsilon_p \frac{\partial C_d}{\partial r}\right)_{r=R} = u^* C_d(R,z). \tag{2-5}$$

In Equation (2-5), u^* is a characteristic droplet deposition velocity and $u^* C_d$ is the rate of deposition. In order to complete the mathematical formulation of the model, an initial condition must be stated that specifies the droplet concentration at the inlet to the duct. In the case of the stable film model, the liquid film flow rate at the inlet to the duct must also be specified. If the boundary and initial conditions are specified, then Equation (2-2) may be solved and applied to

critical heat flux calculations.

The authors whose works are discussed above claimed some degree of success in correlating experimental critical heat flux data. These data were obtained from complex experimental systems in which entrainment, droplet transport, and evaporation probably occurred simultaneously. It is difficult, therefore, to draw significant conclusions regarding the validity of the two droplet transport formulations that are discussed above.

2.1.5 Summary

The review of the critical heat transfer literature pertaining to the fog flow boiling regime reveals several attempts to develop analytical descriptions of the fog flow regime. Two distinct models of turbulent droplet transport have been proposed to describe the motion of droplets in the turbulent gas phase. The first is a one-dimensional model. According to this model, the rate of droplet transport to the duct walls is proportional to the difference between the bulk droplet concentration and the droplet concentration at the wall. This is the mass transfer coefficient approach to the transport process. The second model is a two-dimensional turbulent diffusion formulation, based on Fick's law representation for the turbulent flux of droplets.

The experiments that have been carried out in critical heat transfer studies have been too complex for the purpose of evaluating the utility of either of the two formulations discussed above. It is difficult, therefore, to make a judgment as to the relative merits of the two approaches in describing the turbulent transport of droplets in the fog flow regime.

2.2 Diffusion of Molecular Species in Turbulent Flow

As a preliminary to the discussion of the turbulent diffusion literature, the reader who is unfamiliar with the terminology of turbulent flow is referred to the Appendix for a brief discussion of some statistical quantities which are used to characterize turbulent flows.

2.2.1 Statistical Description of Turbulent Diffusion

Taylor[10] developed the statistical description of turbulent diffusion. He showed that the diffusion process, in homogeneous turbulence, may be described in terms of the motion of a single "fluid particle." The following relation was established between the mean square fluid element displacement after diffusion time, t, $\overline{\sigma^2(t)}$, and the Lagrangian turbulent correlation function $R_L(t)$:

$$\overline{\sigma^2(t)} = 2\,\overline{u^2}\int_0^t \int_0^{t'} R_L(\xi)\,d\xi\,dt, \tag{2-6}$$

where $\overline{u^2}$ is the mean square Lagrangian turbulent velocity. The limiting behavior of this expression was obtained. For "small" diffusion times

$$\overline{\sigma^2}(t) = \overline{u^2}t^2. \tag{2-7}$$

For "large" times

$$\overline{\sigma^2}(t) = 2\overline{u^2}T_L t, \tag{2-8}$$

where T_L is the temporal Lagrangian integral scale.

2.2.2 The Eddy-Diffusion Model of Turbulent Diffusion

Boussinesq[11] first introduced the concept of the eddy viscosity for turbulent momentum transfer. The eddy viscosity relates the turbu-

lent Reynolds stresses to the mean velocity. Turbulent diffusion coefficients for the transfer of heat and mass have been similarly defined. In general, the turbulent flux, q_p, of an arbitrary property with mean value P is given by

$$q_p = -\varepsilon \nabla P, \tag{2-9}$$

where ε is the eddy diffusion coefficient for property P. With this assumption, the conservation equation for property P is

$$\frac{\partial P}{\partial t} + \vec{U} \cdot \nabla P = \nabla \cdot [(D_p + \varepsilon) \nabla P], \tag{2-10}$$

where $\vec{U}$ is the mean fluid velocity and D_p is the molecular diffusion coefficient for property P.

Einstein,[12] in his paper on Brownian motion, showed that one consequence of the diffusion equation

$$\frac{\partial P}{\partial t} = D_p \frac{\partial^2 P}{\partial y^2} \tag{2-11}$$

as applied to a spatially uniform medium, is a relation between the diffusion coefficient and the statistical description of the motion of a single molecule. The diffusion coefficient is given by

$$D_p = \frac{1}{2} \frac{d}{dt} \overline{y^2(t)}, \tag{2-12}$$

where $\overline{y^2(t)}$, the mean square molecular displacement after diffusion time t, is

$$\overline{y^2(t)} = \frac{\int_{-\infty}^{+\infty} y^2 P(y,t)\,dy}{\int_{-\infty}^{+\infty} P(y,t)\,dy} . \qquad (2\text{-}13)$$

For large diffusion times, Einstein showed that D_p is constant.

Dryden[13] applied a diffusion analysis to turbulent mixing in homogeneous, isotropic turbulence in analogy with molecular diffusion. For turbulent transport, however, the displacement of "fluid particles" is considered instead of molecules. Dryden showed, citing Taylor's previous work, that the turbulent diffusion coefficient is constant (independent of time) for large diffusion times. Consequently, he argued, the turbulent diffusion equation

$$\frac{\partial P}{\partial t} = \varepsilon \frac{\partial^2 P}{\partial y^2} \qquad (2\text{-}14)$$

with

$$\varepsilon = \frac{1}{2} \frac{d}{dt} \overline{\sigma^2(t)}, \qquad (2\text{-}15)$$

is a valid representation for large diffusion times. In Equation (2-15), $\overline{\sigma^2(t)}$ is the mean square fluid particle displacement. Batchelor[14] assumed, citing experimental evidence, that the probability density function for particle displacement is Gaussian for all diffusion times. As a consequence he showed that Equation (2-14) is valid for all diffusion times.

The validity of the turbulent diffusion formulation, as applied to homogeneous, isotropic turbulence, has been confirmed by many experiments.[16,17,18,19] In these experiments, measurements of either temperature or tracer-gas concentration were made downstream from either a source of heat or mass. Statistical information about fluid particle

displacement were obtained by fitting a Gaussian curve to the data, thereby determining the dispersion, $\overline{\sigma^2(t)}$. Equations (2-7), (2-8), and (2-15) were then employed to determine the Lagrangian integral scale, the turbulent velocity and the turbulent diffusion coefficient.

The turbulent diffusion model has been applied to flow fields that are not homogeneous (the case for most engineering applications) by allowing the diffusion coefficient to vary spatially and by introducing a dependence on coordinate direction. Since local momentum diffusivity data are generally more common than heat or mass diffusivity data, one assumption commonly made in engineering practice is that the ratio of the thermal (or mass) diffusivity to momentum diffusivity is unity.[20]

2.2.3 Summary

The review of the turbulent diffusion literature shows that the eddy diffusion model, as applied to the diffusion of molecular size species and heat, has been clearly defined. Experiments in nearly homogeneous, isotropic turbulence have proved the validity of the eddy diffusion model in describing the turbulent diffusion process. The diffusion model has proved useful in engineering applications where the turbulence is neither homogeneous or isotropic. The relationship of the diffusion model to Taylor's statistical theory of turbulence has been established. Taylor's analysis, however, is difficult to use in practice because of the difficulty in specifying the form of the Lagrangian correlation function.

2.3 Diffusion of Particulate Matter in Turbulent Flow

2.3.1 Analytical Investigations

The turbulent diffusion model may be formally applied to the

transport of particulate matter, including liquid droplets. A diffusion equation may be written for particulate matter (or discrete particle) concentration and the particle diffusivity may be associated with the mean square particle displacement. Taylor's work remains valid for the motion of discrete particles if, in Equation (2-6), the fluid particle velocity is replaced with that of the discrete particle. The question then arises as to how one may analytically characterize or experimentally measure this diffusivity. The literature pertinent to this question is reviewed below.

The particle diffusivity is defined by

$$\varepsilon_p = \frac{1}{2} \frac{d}{dt} \overline{\sigma_p^2(t)}. \qquad (2\text{-}16)$$

The problem in applying Taylor's work to the calculation of $\overline{\sigma_p^2}$ is the difficulty in obtaining information about the Lagrangian particle correlation function. Attempts have been made to relate Eulerian fluid statistical data, which may be obtained with relative ease, to Lagrangian particle statistics, which are of interest in diffusion calculations.

The analytical approach to this problem has been to formulate equations of motion for a single representative particle, placed in a turbulent fluid. The solution to the equations would, given the necessary fluid velocity data, yield trajectory information about the particle. In principle $\overline{\sigma_p^2}$ and, hence, ε_p could be calculated.

Equations of motion for a particle in a fluid at rest were written independently by Basset, Boussinesq and Oseen.[21,22] These equations were subsequently modified by Tchen,[23] who considered a particle in a spatially uniform velocity field. Lumley[24] generalized these

equations, considering a particle in nonuniform turbulent flow. Whereas Tchen's equations are linear, those developed by Lumley are nonlinear. The nonlinearity of Lumley's formulation arises because of the dependence of the Eulerian velocity on the particle position. The conditions under which the linear and nonlinear theories lead to significantly different results have not been established.

Several authors[25,26,27,28] have used the linear theory as a basis for calculating statistical quantities pertaining to particle motion. The justification often given for employing the linearized equations is that the particle is assumed surrounded by the same fluid eddy at all times. The validity of this assumption, related to the appearance of the particle position in Lumley's formulation, has not been established.

Consider a particle travelling in a spatially uniform turbulent fluid. The turbulent motion is composed of velocity fluctuations with a continuous spectrum of frequencies. The linear theory predicts the following general picture of particle motion: At low frequencies, a particle can follow the turbulent fluid fluctuations; the relative velocity between particle and surrounding fluid is small. At large frequencies the particle lags behind the fluid because of its inertia. It has been shown[23] that the diffusivity (particle or fluid) for large diffusion times depends on the low frequency range of the frequency spectrum. At this end of the spectrum, the particle and fluid act nearly identically. A consequence of the linear model, therefore, is the equality of the fluid and particle diffusivities. One might intuitively expect this theory to be valid for particles whose response times are much less than the smallest time scale of the turbulence. In

addition, the linear theory predicts that the turbulent velocity of a particle is less than that of the fluid, and that the Lagrangian particle integral scale is greater than that of the fluid.

Lumley's work on the nonlinear model is discussed in detail in Chapter III. Briefly, however, he reduced the equations of motion to a nonlinear, stochastic integral equation. Though simplified, the equation still contains the particle position as a parameter in the Eulerian fluid velocity representation. The implication of this model is that, contrary to the assumption inherent in the linear theory, a particle "passes through" eddy after eddy, encountering different fluid elements along its path. Although Lumley discussed an approach to the solution of the equation, results for physically significant situations were not obtained.

Peskin[29] calculated the ratio of particle diffusivity to fluid diffusivity, beginning with Lumley's integral equation. The ratio was shown to be a function of the particle time scale, the fluid particle Lagrangian microscale and the Eulerian time microscale. One consequence of Peskin's result is that the ratio of particle diffusivity to fluid diffusivity decreases with increasing Reynolds number. Peskin cited data taken from Soo[30] to qualitatively support his findings. In the opinion of this author, however, these diffusivity data appear qualitatively incorrect. Additional comments about these data are given in the following section.

2.3.2 Experimental Investigations

Two types of experiments have been performed to obtain information about particulate motion in turbulent flow. In the first type of experiment, individual particle trajectories were tracked. Particle

displacements were measured as a function of time and statistical information were inferred therefrom. This technique has been used[30,31,32,33] to determine the particle diffusivity, turbulent intensity, energy spectra, integral scales and microscales, and the correlation function. In the second type of experiment, concentration distributions were measured downstream from a source of particles. The pertinent form of the diffusion equation was then used to extract statistical information about the particle. Particle diffusivity data were obtained in this manner.

In a series of papers[26,30,34-37] Soo and his co-workers described experiments with solid particles in turbulent air flow. In what appears to be the most significant work of this group of papers,[30] they experimentally determined particle diffusivities, particle integral scales, and particle turbulent velocities in turbulent pipe flow. In addition, tracer-gas diffusion experiments were carried out to determine Lagrangian properties of the single-phase flow, including the fluid diffusivity. The particulate experiments were carried out with 100μ-and 200μ-diameter glass beads. The results indicate that the particle diffusivities are significantly less than that of the fluid. The data (Figure 7 in Reference 30) indicate, however, that the diffusivity of a 200μ-particle is greater than that of a 100μ particle. This result is intuitively incorrect, as mentioned in the discussion of Peskin's work, since it is expected that a heavy particle should diffuse less readily than a lighter one. The following additional conclusions are drawn from the data presented in Soo's paper:

1. The fluctuating velocity of the particle is greater than that of the fluid.

2. The particle integral scale is less than that of the fluid.

3. The ratio of particle diffusivity to fluid diffusivity decreases with mean flow Reynolds number.

The first conclusion seems unrealistic, since the particle derives its energy from the fluid. The second contradicts the implications of the linear theory, as discussed in Section 2.3.1. The linear theory does not predict a Reynolds number dependence on the diffusivity ratio. Although several questions have arisen concerning the data presented in this paper, the results, as a whole, are incompatible with the implications of the linear model of particle flow.

Wakstein[38] measured particulate concentration, and mean and fluctuating velocities in turbulent pipe flow of air. The diffusion equation was integrated numerically to calculate local values of the particle diffusivity. Axial particle concentration gradients, necessary for the calculation, were not measured; they were deduced from an independent experiment on the turbulent diffusion of a tracer gas. Neither the air nor particulate flows were fully developed.

Several experiments dealing with the flow of liquid droplets, of particular interest in this research, are considered next.

Alexander and Coldren[39] investigated the transport of droplets in turbulent pipe flow. Experiments were performed in which droplets were injected into the air flow at the center of a 1.86-inch diameter pipe. Impact tubes were employed to sample the liquid phase. The rate of collection of liquid was assumed proportional to the local droplet mass flux. The results indicated to the authors that two regions downstream from the injector should be considered separately. The first, immediately downstream from the injector, showed considerable variation

of mass flux across the pipe diameter. It was proposed that in this region the turbulent diffusion process in the central region of the pipe controls the transport process. The eddy diffusion model was applied to this region, with the assumption of zero droplet concentration at the wall. The second region, further downstream from the injector, showed a relatively uniform mass flux distribution across the pipe diameter. Alexander and Coldren proposed that the droplet transport process in this region is controlled by the relatively stagnant film of fluid near the wall. The mass transfer coefficient formulation was used to describe the droplet transport process in this region. The authors used the droplet flux data to determine droplet diffusivities and mass transfer coefficients.

In the opinion of this author, the major drawbacks to the work of Alexander and Coldren are:

1. The air velocity through the air-atomizing nozzle, which was used as droplet generator, was about 800 ft/sec; the mean air velocity in the pipe was 100-200 ft/sec. Thus, the region just downstream from the droplet injector had mean and turbulent velocity properties which were probably markedly different from fully developed turbulent pipe flow characteristics. The diffusivities extracted from the data cannot, therefore, be interpreted as applying to pipe flow conditions.
2. The droplets emerging from the nozzle had velocities considerably above the mean flow velocity. They did not decelerate to their steady state velocity in the 67 inches downstream from the source in which the diffusivities were determined.
3. The droplet size distribution generated by the nozzle was not

determined. An estimate of the mean drop size was made, however, based on previous experience with the nozzle.

Based on the previous discussion, it is concluded that the particle diffusivity data obtained by Alexander and Coldren are not characteristic of fully developed turbulent pipe flow. The significance of this data is, therefore, questionable.

Longwell and Weiss[40] measured droplet mass flux distributions downstream from a point source of droplets in turbulent pipe flow. The stream was sampled with an impact probe at an axial position 35 inches from the droplet source. The major objections to this work are:

1. No information was presented regarding the nature of the droplet source or the size droplets.
2. The turbulent air flow was not fully developed.
3. Air velocities were about 300 ft/sec, whereas the droplet injection velocity was 7.5 ft/sec. The droplets had not accelerated to their steady state velocities in the 35 inches from the source in which the measurements were made. The diffusivity was not constant with axial distance.

The point source solution of the diffusion equation fits the concentration data well. The diffusivity information, however, are not properties of fully developed turbulent pipe flow. The significance of the diffusivity data is, therefore, questionable.

Stein et al.[9] described an attempt to use a photographic technique to measure droplet concentration distributions downstream from a point source of water droplets in a turbulent pipe flow of steam. A limited number of experiments were carried out with the droplets confined to the central region of the pipe. The turbulent diffusion model was

proposed to describe the droplet transport process. Particle diffusivity information was extracted from the data. On the basis of photographic evidence, however, it was speculated that the diffusivity data might be erroneous because of possible injector nozzle vibration. This investigation was meant to be preliminary to a more definitive study, which did not materialize at the time.

Goldschmidt and Eskenazi[41] used a hot wire anemometer to measure liquid droplet mass flux distributions in the similarity region of a two-dimensional turbulent jet. The air velocity and particle concentration distributions were shown to be self-similar. The droplet size distribution was measured; the mean droplet size was 2.2 microns with a standard deviation of 3.3 microns. It was found that the ratio of particle diffusivity to fluid diffusivity was 0.9. This indicates that the results of the linear theory of the particle dynamics problem is approximately valid for the droplet size range and flow parameters considered by Goldschmidt and Eskenazi.

2.3.3 Summary

The review of the literature pertinent to particulate motion in turbulent flow reveals a scarcity of available data. In particular, there are little data describing the particle diffusivity as a function of particle parameters and turbulence properties. The application of the diffusion model to particulate flows of practical interest is, therefore, difficult.

The linear model does not adequately explain the existing data. The data reveal that the particle diffusivity is less than the fluid diffusivity, contrary to the equality of the two predicted by the linear theory. The linear model appears to be approximately valid, however,

for the 2.2μ droplets in the turbulent plane jet described by Goldschmidt and Eskenazi.

Although the approach taken by Lumley[24] holds some promise of overcoming the shortcomings of the linear theory, only Peskin[29] has attempted to pursue the approach. There are insufficient particle diffusivity data appearing in the literature to assess the validity of Peskin's result.

III. ANALYTICAL CONSIDERATIONS

In this chapter the conservation of mass equation is applied to droplet transport in turbulent pipe flow. The turbulent diffusion model is defined and the implications of the model are discussed.

Lumley's nonlinear equations of particle motion are discussed and a solution to the equations is obtained for the case of large particle terminal velocity. For this case, an expression for the particle diffusivity is obtained.

3.1 Droplet Transport Model

3.1.1 The Conservation of Mass Equation

The mass conservation equation for droplets flowing in a fluid with convective velocity $\vec{V}$ may be written

$$\frac{\partial C^*}{\partial t} + \vec{V} \cdot \nabla C^* = S, \tag{3-1}$$

where C^* is the local droplet mass concentration and S is the droplet source (or sink) term.

For the flow of droplets in a turbulent gas, let

$$C^* = C + c$$

$$\vec{V} = \vec{V}_p + \vec{v}, \tag{3-2}$$

where C are $\vec{V}_p$ and the temporally averaged droplet concentration and convective velocity; respectively, and c and $\vec{v}$ are the corresponding fluctuating quantities. Insert Equations (3-2) into Equation (3-1) and time average the result. Consider the region away from droplet sources. For the stationary-state case, the resu

$$\vec{V}_p \cdot \nabla C + \nabla \cdot \overline{\vec{v}c} = 0. \qquad (3\text{-}3)$$

The quantity $\overline{\vec{v}c}$ represents the turbulent flux of droplets in the three coordinate directions. The over-bar denotes a time average.

3.1.2 The Turbulent Diffusivity Formulation

Equation (3-3) contains two dependent variables: the mean concentration, and the turbulent flux of droplets. The turbulent diffusivity formulation provides a relation between the two quantities.

The particle diffusivity is defined by

$$\overline{\vec{v}c} = -\varepsilon_p \nabla C \qquad (3\text{-}4)$$

This expression is a relationship between the local concentration gradient and the local turbulent flux of droplets. In general, ε_p is a function of coordinate direction and position. If ε_p is dependent on coordinate direction, then the diffusivity is a tensor quantity.[14] In addition, ε_p is expected to depend on fluid turbulence characteristics and particle parameters.

Consider the flow of droplets in fully developed turbulent pipe flow. Assume that the droplet concentration distribution is azimuthally symmetric and that axial diffusion is negligible. The transport equation for this case is

$$V_p \frac{\partial C}{\partial z} = \frac{1}{r} \left(r\varepsilon_p \frac{\partial C}{\partial r} \right), \qquad (3\text{-}5)$$

where V_p is the scalar mean axial velocity. For the case V_p a constant, and ε_p a constant, Equation (3-5) is recognized as the classical diffusion equation. For this case, Equation (3-4) is the Fick's law diffu-

sion formulation. Equations (3-5) and (2-16) represent the link between the Eulerian description of the droplet flow field and the Lagrangian statistical description of particulate motion. If the Eulerian quantities are measured, the above relations may be used to draw inferences about the Lagrangian particle statistics. This was the approach taken in the experimental portion of this investigation.

3.1.3 Droplet Transport in the Central Core Region of Turbulent Pipe Flow

Experiments have shown that turbulence in the central core region of turbulent pipe flow is nearly homogeneous and isotropic.[50] Hinze[44] showed that the turbulent momentum flux may be characterized by a constant eddy viscosity in this region. Heat and mass transfer studies have shown similar behavior for the eddy conductivity and turbulent mass diffusivity.[43] There is some justification, therefore, in presuming that the particle diffusivity is independent of radius in the central core region of pipe flow. It is also reasonable to assume that the mean droplet velocity in this region is uniform.[38]

For a droplet falling in the same direction as that of the gas flow, the mean droplet velocity is

$$V_p = U_o + u_t,$$

where U_o is the mean gas velocity at the pipe center and u_t is the particle terminal velocity. Let

$$E_p = \varepsilon_p / V_p. \tag{3-6}$$

Equation (3-5) becomes

$$\frac{1}{E_p}\frac{\partial C}{\partial z} = \frac{1}{r}\frac{\partial}{\partial r}\left(r\frac{\partial C}{\partial r}\right). \qquad (3\text{-}7)$$

The assumption of radially independent diffusivity implies a diffusion model for turbulent transport. A diffusion model implies that the length scale of the process responsible for the transporting is much less than the characteristic dimensions of the fluid-medium boundaries. Although this is generally true for the molecular diffusion process, it is not necessarily the case for turbulent transport. In turbulent pipe flow, for example, the characteristic dimension of the eddies doing the transporting is of the same order of magnitude as the pipe diameter. The assumption of uniform diffusivity is made, however, recognizing that experiments must show how reasonable a description it represents of the transport process.

The solution to Equation (3-7) for a plane source of droplets, S(r), located at z = 0 is required. This problem is mathematically equivalent to the heat conduction problem for the temperature in an infinite medium with an initial radially symmetric temperature distribution. The solution[45] as applied to the present problem is

$$\frac{C(r,z)}{CMAX} = \frac{\int_0^\infty S(r')r'dr' I_o\left(\frac{rr'}{2E_p z}\right) \exp\left[-\frac{(r^2 + r'^2)}{4E_p z}\right]}{\int_0^\infty S(r')r'dr' \exp\left[-\frac{r'^2}{4E_p z}\right]} \qquad (3\text{-}8a)$$

$$\equiv \phi_1(r,z),$$

where CMAX = C(0,z), I_o is the zeroth order modified Bessel Function, and z is the axial distance from the plane source.

For a point source of droplets, the solution to Equation (3-7)

is the Gaussian

$$\frac{C(r,z)}{CMAX} = \exp\left(-\frac{r^2}{4E_p z'}\right) \qquad (3\text{-}8b)$$

$$\equiv \phi_2(r,z'),$$

where z' is the axial position from the point source.

3.2 The Motion of Discrete Particles in Turbulent Flow

3.2.1 The Equations of Motion for a Particle in Turbulent Flow

Basset, Boussinesq and Osseen[22,23] developed the equation for the net drag force acting on a spherical particle moving through a fluid at rest. Using the Stokes' approximation for the drag on a sphere, the particle momentum equation is

$$\frac{4}{3}\pi a^3\rho_p\dot{v}_i = -\frac{2}{3}\pi a^3\rho_f\dot{v}_i - 6\pi\mu a\left[v_i + \frac{a}{\sqrt{\pi\nu}}\int_0^t d\tau\,\frac{\dot{v}_i(\tau)}{\sqrt{t-\tau}}\right]$$

$$-\frac{4}{3}\pi a^3(\rho_p - \rho_f)\,g_i \qquad (i = 1,3), \qquad (3\text{-}9)$$

where v_i is the ith component of the particle velocity, and the dot represents time differentiation.

The first term on the right side of Equation (3-9) describes the apparent mass effect. This term represents the force required for a perfect fluid to accelerate the sphere. The second term is the sum of the steady state Stokes' drag force and the unsteady, viscous drag force which arises out of particle acceleration. The last term is the gravitational force acting on the particle, which acts in the ith coordinate direction.

Tchen[23] wrote Equation (3-9) for a particle in a uniform fluid velocity field $u_i(t)$. Corrsin and Lumley[46] rewrote the equation of motion for a particle in a nonuniform velocity field $u_i(x_j,t)$. The equation as given by Hinze[23] is

$$\frac{d}{dt} v_i = \frac{3\rho_f}{2\rho_p + \rho_f} \left[\frac{d}{dt} u_i - 2/3\, \nu \frac{\partial^2 u_i}{\partial x_j \partial x_j}\right]$$

$$+ \frac{2}{2\rho_p + \rho_f} \left\{\frac{18\mu}{d^2} [u_i - v_i] + \rho_f [u_k - v_k] \frac{\partial u_i}{\partial x_k}\right\}$$

$$+ \frac{18}{(2\rho_p + \rho_f)d} \sqrt{\frac{\rho_f \mu}{\pi}} \int_{t_o}^{t} dt' \frac{\frac{d}{dt}[u_i - v_i]}{\sqrt{t - t'}}, \quad i = 1,3, \qquad (3\text{-}10)$$

where the Eulerian velocity $u_i(x_j,t)$ is interpreted as the fluid velocity at the instantaneous particle position. The term du_i/dt is the derivative of the fluid velocity, following the motion of a particle. The Einstein subscript convention is used in Equation (3-10).

Equation (3-10) is a nonlinear, second order differential equation. The equation is nonlinear on two accounts. First, Equation (3-10) contains the nonlinear inertial terms characteristic of the Navier-Stokes' equations. The second cause of the nonlinearity is the appearance of the particle position in the Eulerian velocity function u_i. Neither of these nonlinearities appear in Tchen's formulation of the problem.

Lumley[24] investigated the implications of the second type of nonlinearity, i.e., the appearance of the particle position in the fluid velocity expression. A simplified version of Equation (3-10) was

studied. Lumley assumed that:

(a) The Eulerian flow field is homogeneous, isotropic, incompressible and stationary.

(b) The particle diameter is smaller than the smallest length scale of the turbulent flow.

(c) The time scale of the particle is smaller than the smallest time scale of the turbulence.

With these assumptions, Lumley reduced the equations of motion to

$$\sigma_{pi}(a_k,t) = a_i + \int_0^t G(t-\tau)u_i\,[\sigma_{pj}(a_k,\tau),\tau]d\tau, \tag{3-11}$$

where $u_i(\sigma_{pj},t)$ is the Eulerian fluid velocity at the particle position σ_{pj}. In addition,

$$G(t) = 1- \exp\,(-t/T), \tag{3-12}$$

where T, the particle response time, is

$$T = \frac{a^2(2\,\frac{\rho_p}{\rho_f} + 1)}{9\nu}\,. \tag{3-13}$$

Equation (3-11) may be written in the equivalent differential form:

$$T\,\frac{d^2\sigma_{pi}}{dt^2} + \frac{d\sigma_{pi}}{dt} = u_i(\sigma_{pj},t). \tag{3-14}$$

As discussed in Section 2.3.1, this equation, in its linear form (u_i time dependent only), has been studied by several authors.

Equation (3-11) is a nonlinear, stochastic integral equation.

The Eulerian field $u_i(x_j,t)$ is the given quantity. The solution to this equation is the description of the motion of a particle in terms of the Lagrangian coordinates, σ_{pi}. Lumley[24] discussed an approach to the solution of this equation. Further study by this author of Lumley's work is required to meaningfully assess his analysis.

3.2.2 Case of Large Particle Terminal Velocity

Consider a particle with large terminal velocity. Assume that the particle falls through turbulent eddies. This assumption is conceptually different from the assumption of the linear model, in which a particle is considered retained in a single eddy throughout its history. For this case, Equation (3-11) is

$$\sigma_{pi}(t) = \int_0^t G(t-\tau)u_i[\sigma_{pj}(\tau),\tau]d\tau + u_t t\delta_{3i} \qquad (3\text{-}15)$$

where $i = 3$ is the direction of particle free fall, δ_{ij} is the Kronecker delta, and u_t is the particle terminal velocity given by

$$u_t = \frac{(\rho_p - \rho_f)}{18\mu} d^2 g. \qquad (3\text{-}16)$$

Note that $T = u_t/g$ for large ρ_p/ρ_f.

For $i = 2$, a coordinate perpendicular to the free fall direction, Equation (3-15) is

$$\sigma_{p2}(t) = \int_0^t G(t-\tau)v(\sigma_{p1},\sigma_{p2},\sigma_{p3} + u_t\tau,\tau)d\tau. \qquad (3\text{-}17)$$

In Equation (3-17) $v = u_2$.

Assume that the terminal velocity of the particle is much greater

than the turbulent fluctuating velocity, i.e.,

$$v/u_t << 1.$$

For this case, the distance $u_t t$ travelled in the i = 3 direction is considerably greater than the distances σ_{pi} travelled in response to the turbulent fluid fluctuation, i.e.,

$$\sigma_{pi} << u_t t.$$

Let $\eta = u_t \tau$. For large u_t, the component of the Eulerian fluid velocity transverse to the free fall direction becomes

$$\lim_{u_t \to \infty} v(\sigma_{p1},\sigma_{p2},\sigma_{p3} + u_t\tau,\tau) = \lim_{u_t \to \infty} v(\sigma_{p1},\sigma_{p2},\sigma_{p3} + \eta,\eta/u_t)$$

$$= v(0,0,\eta,0). \qquad (3\text{-}18)$$

On defin

$$v(0,0,\eta,0) \equiv v(\eta) = v(u_t\tau),$$

Equation (3-17) becomes

$$\sigma_{p2}(t) = \int_0^t [1 - \exp(-\frac{t-\tau'}{T})]\, v(u_t\tau')d\tau'. \qquad (3\text{-}19)$$

The mean square particle displacement is

$$\overline{\sigma_{p2}^2(t)} = \int_0^t \int_0^t [1-\exp(-\frac{t-\tau'}{T})][1-\exp(-\frac{t-\tau''}{T})]$$

$$\times \overline{v(u_t\tau')v(u_t\tau'')}\, d\tau' d\tau'' . \qquad (3\text{-}20)$$

Let $\eta = u_t t$, $\eta' = u_t \tau'$, and $\eta'' = u_t \tau''$. Define the transverse Eulerian correlation function, R_{22}, as

$$\overline{v^2}\, R_{22}(\eta' - \eta'') = \overline{v(\eta')v(\eta'')} \quad . \tag{3-21}$$

Equation (3-21) implies that the turbulence is homogeneous. Equation (3-20) becomes

$$\overline{\sigma_{p_2}^2(t)} = \frac{\overline{v^2}}{u_t^2}\int_0^{u_t}\int_0^{u_t} [1-\exp(-\frac{\eta-\eta'}{u_t t})][1-\exp(-\frac{\eta-\eta''}{u_t t})]$$

$$\times\, R_{22}(\eta' - \eta'')d\eta' d\eta'' \tag{3-22}$$

A functional form for R_{22} must be chosen in order to evaluate this integral. Assume that[47]

$$R_{22}(\xi) = (1-\xi/2L_E)\exp(-\xi/L_E) \quad . \tag{3-23}$$

The function $R_{22}(\xi)$ is the transverse correlation function which, in isotropic turbulence, corresponds to the longitudinal correlation $\exp(-\xi/L_E)$. In Equation (3-23), L_E is the Eulerian integral scale

$$L_E = \int_0^\infty \exp(-\xi/L_E)d\xi.$$

The particle diffusivity is defined by

$$\varepsilon_p = \frac{1}{2}\frac{d}{dt}\overline{\sigma_{p_2}^2(t)} \quad . \tag{3-24}$$

Insert Equation (3-23) into Equation (3-20) and the result into Equation

(3-24). The particle diffusivity, for large diffusion time is[47]

$$\varepsilon_p = \frac{L_E}{2u_t} \overline{v^2} \ . \qquad (3\text{-}25)$$

IV. EXPERIMENTAL INVESTIGATION

The major objective of the experimental investigation was to test the validity of the Fick's Law description of turbulent droplet transport, as applied to a region of spatially uniform turbulence. The second objective was to investigate the dependence of the particle diffusivity on the particle terminal velocity and on the flow characteristics of the turbulent fluid. The central core region of fully developed pipe flow was chosen to approximate a spatially uniform turbulent flow field.

4.1 Experimental Approach

The motion of a particle in a turbulent fluid is determined by the statistical properties of the turbulence and by the particle characteristics. The experimental investigation, therefore, was carried out in two parts: First, a study was made of the properties of the turbulent, single phase air flow; second, a study was made of droplet transport in turbulent pipe flow.

4.1.1 Air Flow Measurements

The air flow measurements were carried out to satisfy two objectives:

(1) To determine whether the properties of the air flow were independent of axial distance along the pipe.

(2) To establish the mean velocity and turbulent intensity characteristics of the air flow.

These measurements were carried out with a hot wire anemometer.

4.1.2 Droplet Flow Measurements

The objectives of the droplet flow experiments were:

(1) To test the validity of the turbulent diffusion model, as applied to droplet transport in a region of approximately uniform turbulence.

(2) To measure the particle diffusivity as a function of particle terminal velocity and turbulent flow characteristics.

The approach taken in this portion of the experimental study is analogous to the approach employed in previous investigations of turbulent diffusion of heat and molecular size species. These investigations are briefly discussed in Section 2.2.2.

Uniform size droplets were introduced into the flow at the center of the pipe. The droplets flowed vertically downward, concurrently with the air flow. Droplet concentration distributions were measured at several axial positions downstream from the droplet injector. Equation (3-8a) describes the droplet concentration distribution downstream from an arbitrary, axially symmetric source of droplets. The distributions measured downstream from the source of droplets were fitted to Equation (3-8a), using a least squares fitting procedure.[49] This procedure yielded a value of the particle diffusivity for each position downstream from the source, and for each set of droplet and flow parameters.

The droplet concentration measurements were carried out with a hot wire anemometer.

4.2 Description of Apparatus

4.2.1 Experimental Design Criteria

The experimental apparatus was designed to meet the following general requirements:

(1) To ensure fully developed pipe flow conditions at the site of the droplet flow experiments.

(2) To allow as large a region as possible away from the pipe walls for the droplet concentration measurements. In this region the air flow properties and the particle diffusivity were considered uniform.

(3) To inject droplets into the pipe flow with a clearly defined droplet size distribution.

(4) To inject droplets into the flow stream with velocities as close as possible to the sum of the air velocity and droplet terminal velocity.

(5) To minimize the flow disturbance caused by the droplet injector structural members.

4.2.2 Fog Flow Test Facility

A flow facility, shown schematically in Figure 2, was constructed to provide a turbulent field in which to carry out the droplet transport study. Figure 3 is a photograph of the facility.

The duct was fabricated from 6-foot lengths of 7 1/2-inch diameter commercial Lucite tubes. The tubes were vertically stacked to a total height of 38 feet. Each 6-foot section was provided with a set of Lucite flanges machined with O-ring grooves. A neoprene O-ring was inserted into each groove. This provided the seal between sections. The tubes were tapered at the ends of the sections to ensure against abrupt changes in the inside diameter, as the air flowed from one tube to another.

A centrifugal blower, driven by a 5-horsepower, constant speed motor, was situated at the base of the duct. The blower delivered up to 600 cubic feet per minute of air into the system, equivalent to a maximum mean flow Reynolds number of 100,000. The air flow rate was control-

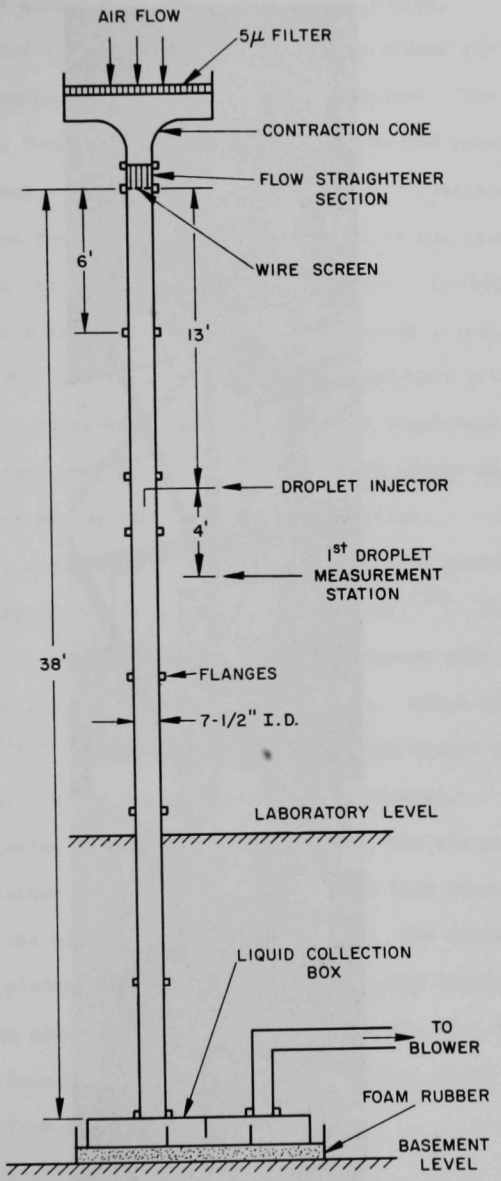

Fig. 2. Schematic of Flow Facility

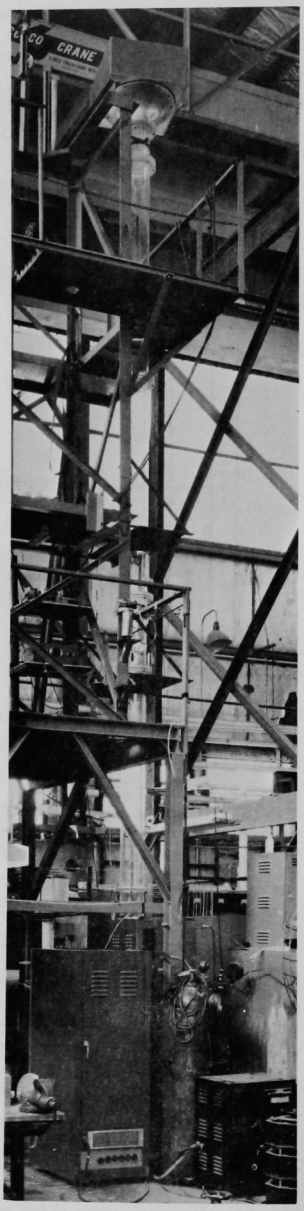

Fig. 3. Photograph of Flow Facility

led by means of a gate placed downstream of the blower.

Air entered the system at the top of the column and flowed into a 26"x26"x12" chamber, containing a fiberglass filter. The filter, rated 95% efficient for 5-micron-diameter particles, removed particlate solids from the air stream. The air then passed through a contraction cone, with a contraction ratio of 3 to 1. The purpose of the cone was to provide a "smooth" entry of air into the flow tube. Following the contraction cone was a one-foot-long flow-straightening section. This section was composed of 3/4-inch inside diameter, 1/8-inch wall thickness, Lucite tubes. The tubes were cemented into, and completely filled, the 7-1/2-inch-diameter outer Lucite tube. A 24-mesh screen was placed at the downstream end of the flow straightening section.

The entry section to the flow tube discussed above was designed in a manner analogous to the design used by Laufer.[50] The purpose of this design was to attain a fully developed turbulent pipe flow in a minimum length of pipe downstream from the entry. Other designs have been proposed,[51,52] but were not used, since the author did not become aware of them until after the equipment was fabricated.

After flowing through the test facility, the air passed through an aluminum container located at the base of the flow tube. The air exhausted through the blower into the environment. The container housed a set of baffle plates, which served to separate the liquid from the flow stream. The aluminum container, upon which the flow tube was mounted, rested on a 3-inch-thick cushion of foam rubber, which served to absorb vibrations from the blower

4.2.3 Liquid Supply System

To avoid plugging the small capillary tubes employed in the drop-

let production apparatus, it was necessary that the liquid used in the experiment be free of solid contaminants. It was required that the liquid storage and supply system be kept extremely clean, and be constructed of noncorrosive materials.

Distilled water was used in the droplet flow experiments. Stainless steel was used in all liquid supply system apparatus. Copper tube was used in all connecting lines. Valves were constructed of stainless steel and brass.

A schematic of the liquid supply system is shown in Figure 4. The water was stored in a stainless steel vessel, which was hydrostatically pressure tested to 1000 psi. The vessel held 6 gallons of liquid. A helium gas bottle, connected to the storage vessel, supplied the pressure (up to 400 psi) to feed the liquid through the system. The water flowed out of the storage vessel and through a 3-micron particle diameter filter. The filter was installed to ensure that any particulate matter in the system did not reach the capillary tube. After leaving the filter, the water passed through a metering valve designed to control liquid flow rates up to 34 cc/min. A Brooks Instrument Company Rotameter, Model 2-FV-1110-6, was employed to measure the liquid flow rate. The rotameter tubes were designed for liquid flow rates of 2-20 cc/min and 0.6-2.0 cc/min. Measurements of liquid flow rate were made with $\pm$2% full scale accuracy. After leaving the rotameter, the liquid flowed through another filter and from there to the droplet injection system.

4.2.4 Droplet Production System

The choice of a droplet injection system was subject to the following requirements:

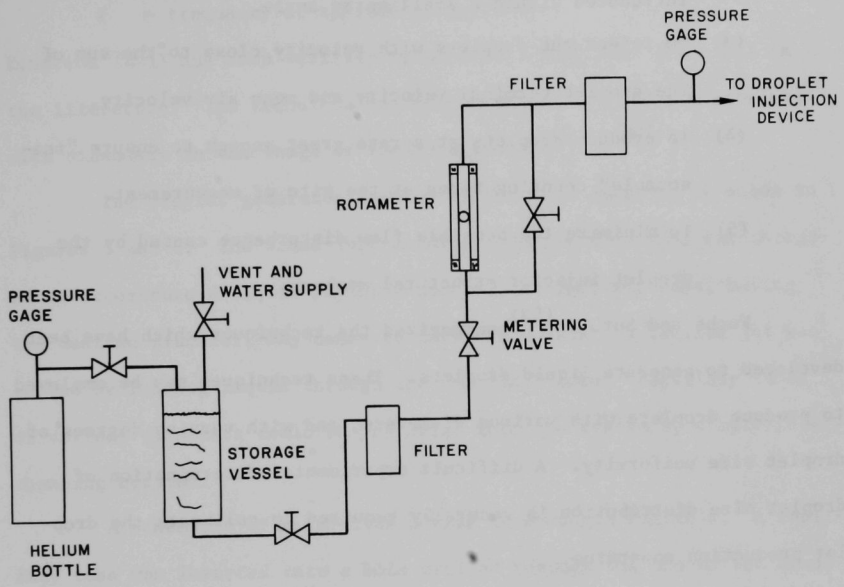

Fig. 4. Liquid Supply System

(1) To introduce into the air stream a source of liquid droplets with a well defined droplet size distribution.

(2) To confine the stream of droplets to the central core region of the pipe. This required that the droplets be introduced within a small spray angle.

(3) To inject the droplets with velocity close to the sum of the droplet terminal velocity and mean air velocity.

(4) To produce droplets at a rate great enough to ensure "reasonable" counting times at the site of measurement.

(5) To minimize the possible flow disturbance caused by the droplet injector structural members.

Fuchs and Sutugin[53] summarized the techniques which have been developed to generate liquid droplets. These techniques may be employed to produce droplets with various diameters, and with varying degrees of droplet size uniformity. A difficult experimental determination of droplet size distribution is generally required to calibrate the droplet production apparatus.

The technique chosen to satisfy the above requirements takes advantage of the natural instability of a laminar liquid jet. Raleigh[54] showed that a liquid jet is unstable, under the action of surface tension, with respect to disturbances of wavelengths greater than the circumference of the jet. If a disturbance of the proper wavelength is applied to a liquid jet, the jet is broken into a stream of uniform diameter droplets. The rate of droplet production is equal to the frequency of the applied disturbance. The droplet diameter is given by

$$d = \left(\frac{6}{\pi}\frac{Q}{f}\right)^{1/3} = \left(6\,\frac{d_o^{\,2} v_o}{f}\right)^{1/3}, \qquad (4\text{-}1)$$

where

v_o = liquid jet velocity

Q = liquid flow rate

d_o = liquid jet diameter

f = frequency of applied disturbance.

Equation (4-1) has been verified in several experiments described in the literature. The technique has been employed to generate droplets with diameters in the range of 25-350 microns.[55,56,57]

The droplet generator section of the flow facility is shown in Figures 5 and 6. The brass tube leading into the flow tube was threaded to accomodate a liquid injector nozzle. A capillary tube, having the desired diameter, was cemented into the nozzle. A laminar jet was formed by forcing liquid through the capillary tube. Capillary tubes of various diameters could be installed into the system by simply interchanging nozzles.

A schematic of an injector nozzle is shown in Figure 7. A capillary tube was inserted into a hole drilled through the tip of the brass holder. The tube was cemented into place with a metal-base epoxy. The bond withstood 400 psi with no evidence of leakage. The nozzles were fabricated with extreme care to keep them free of traces of particulate matter. An O-ring provided the liquid seal between the nozzle and the brass tube. A brass retainer sleeve was placed over the O-ring to keep it in place at the high pressures encountered in the experiments.

Three capillary tubes were employed in the experiments. A 4-mil (100μ) stainless steel hypodermic tube was bought, and two glass capillary tubes were drawn by the Argonne National Laboratory Biology Division Glass Shop. The inside diameters of the glass capillary tubes were

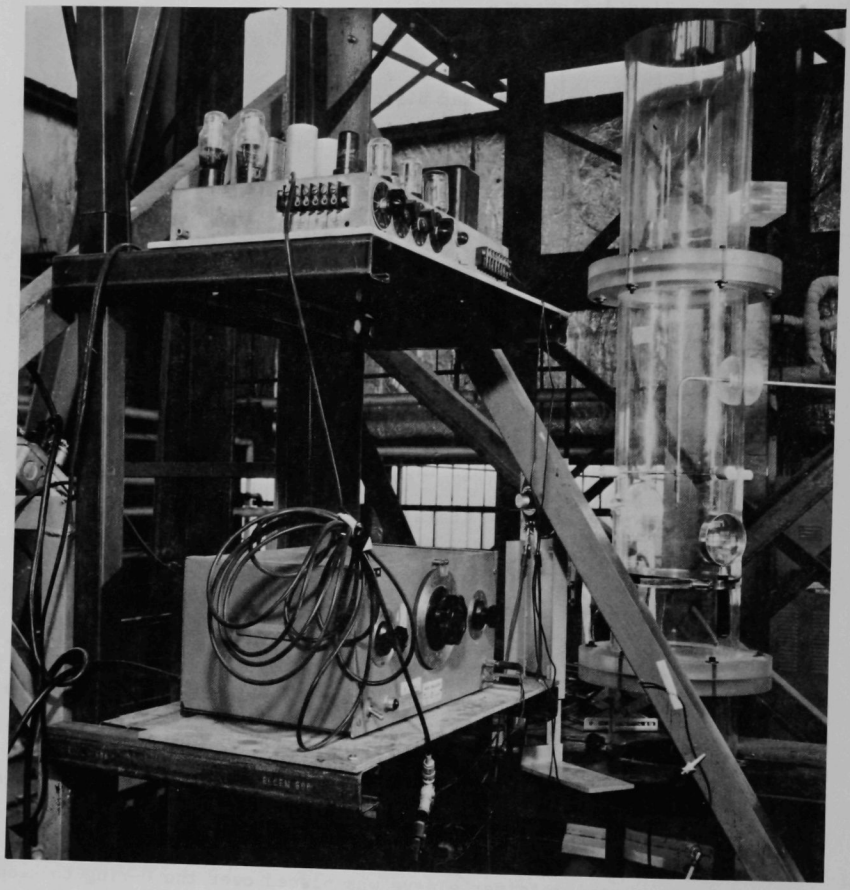

Fig. 5. Droplet Generator Equipment

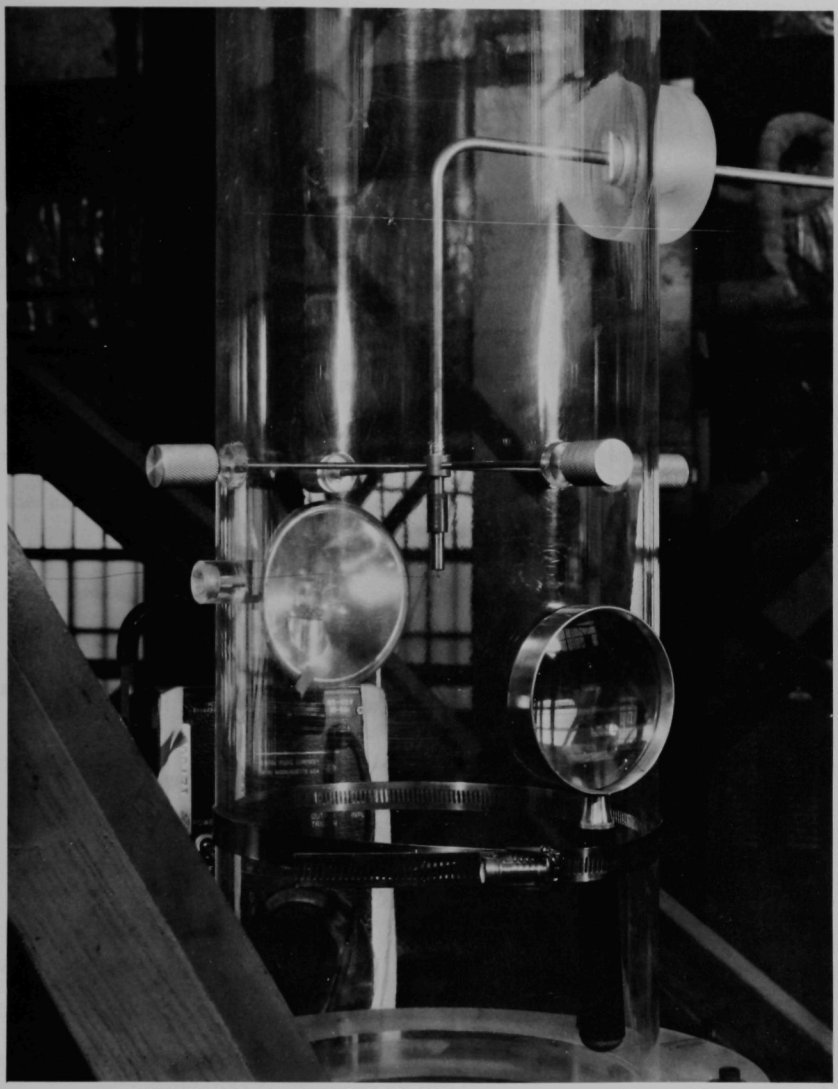

Fig. 6. Droplet Injector Assembly

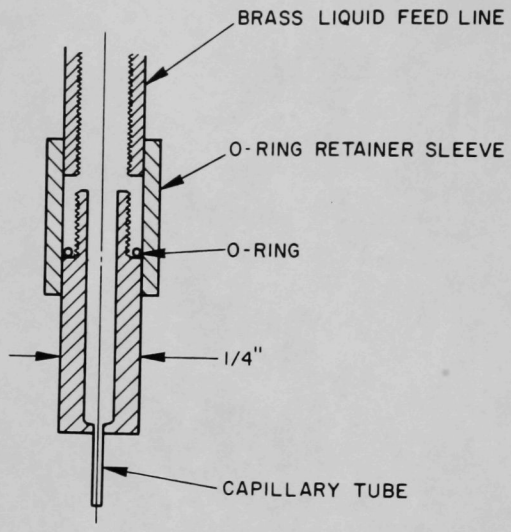

Fig. 7. Droplet Injector Nozzle

50μ and 75μ. The capillary tubes were microscopically inspected to ensure that they were free of burrs. It was found that if a burr was present at the tip of a capillary tube, the liquid jet "followed the burr" and flowed at an angle to the tube.

A disturbance of the desired frequency was applied to the liquid jet in the manner shown schematically in Figure 8. A photograph of the apparatus appears in Figure 5. The oscillator signal was fed into an audio amplifier, which had a peak output of 40 volts. The amplifier output was used to drive a 3.2-ohm speaker. One end of a fine copper wire was cemented to the speaker cone, and the other end to the edge of the capillary tube. A disturbance of the desired frequency was transmitted by the wire to the capillary tube, and hence to the liquid jet, using the speaker as the mechanical driver mechanism.

The smallest diameter droplets that could be produced with the system described above was determined by the following factors:

(1) The combined frequency response of the amplifier and speaker.

(2) The stiffness of the capillary tubes.

(3) The maximum pressure that could be safely applied to the liquid supply system.

As a result of these limitations, frequencies significantly greater than 14kHz could not be applied to the jet. Droplets smaller than 80μ could not be produced. Smaller droplets can be produced, however, by directly coupling a piezoelectric crystal to the capillary tube.[55]

Figure 9 shows a stream of uniform droplets produced by the excitation of the liquid jet emerging from a 8-mil stainless steel hypodermic tube. The droplet diameter, determined from the photograph, was

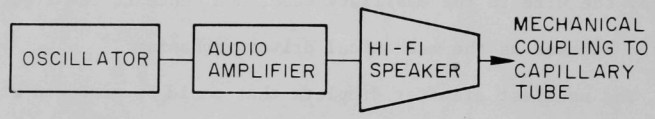

Fig. 8. Jet Perturbation Apparatus

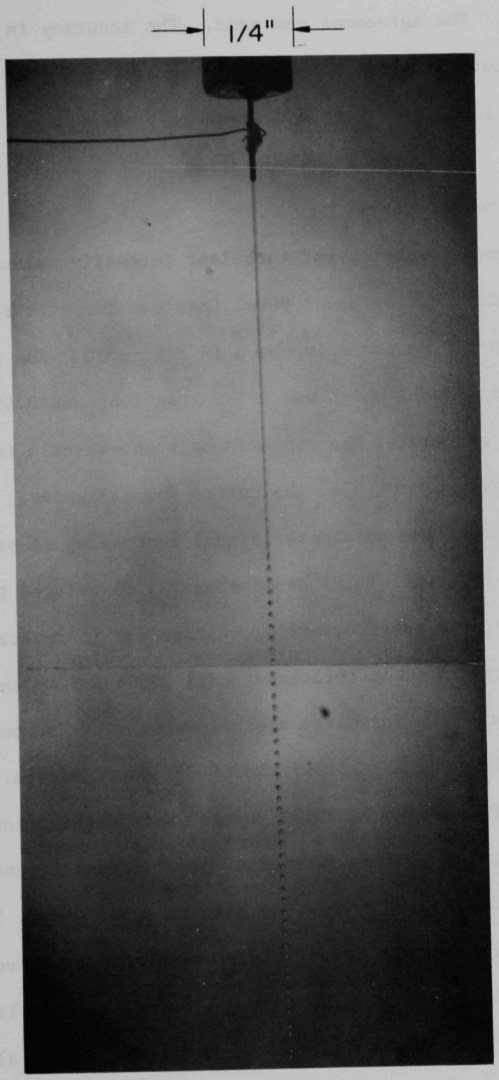

Fig. 9. Droplet Stream from an 8-Mil Hypodermic Tube

350 microns. Equation (4-1) was used to calculate the theoretical droplet diameter. The agreement was good. The accuracy in the measurement of the droplet diameter, governed by the accuracies in the determination of the liquid flow rate and frequency, was ±3%.

4.3 Instrumentation

4.3.1 Air Flow Measurements

Temporal mean velocity and turbulent intensity measurements were made with a Flow Corporation Model 900-1 Constant Temperature Hot Wire Anemometer. The hot wire probe is shown in Figure 10. The probe held a tungsten filament sensor which was 0.1 inches long and 0.00035 inches in diameter. The anemometer was operated at a hot-to-cold resistance ratio of 1.5 during the course of the entire investigation.

A schematic of the anemometer signal processing is presented in Figure 11. The d-c output of the anemometer (E) is related to the local mean flow velocity; the rms fluctuating voltage (e) is related to the turbulent intensity. A Hewlett-Packard Model 3400A RMS Voltmeter was employed in the turbulent intensity measurements. The anemometer signal was visually monitored on a Tektronix Model 549 Oscilloscope.

A Hewlett-Packard Model 2010G "Dymec" Data Acquisition System was employed to convert the instantaneous output signal of the anemometer to digital form and to record the data on paper tape. Two channels of the "Dymec" were used; the first sampled the mean output voltage of the anemometer, and the second sampled a d-c output signal proportional to the rms anemometer output voltage. The two signals were alternately sampled at the rate of one sample per second for 30 seconds, giving 15 records for each quantity measured. The data were fed into a CDC-160A digital computer where they were time averaged, and where the velocities

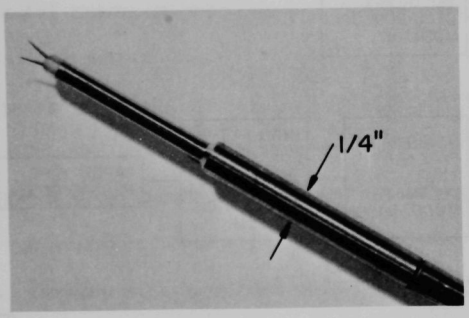

Fig. 10. Hot Wire Sensor

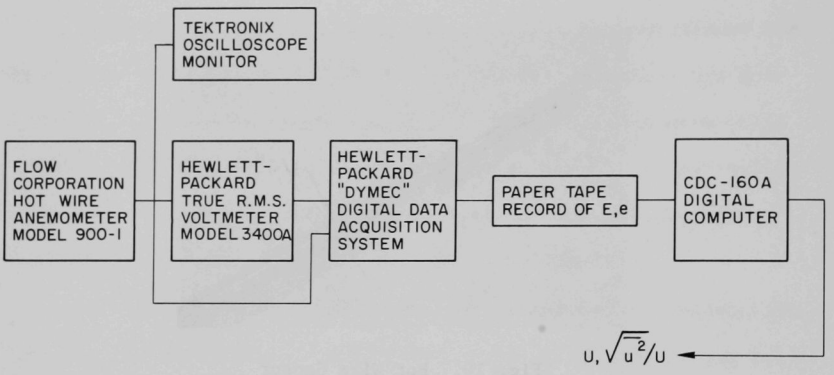

Fig. 11. Anemometer Signal Processing Single Phase Flow

and intensities were computed. The reproducibility of the data was excellent, as shown in Section 5.1.

The hot wire probes were rigidly mounted in the radial traverse mechanisms shown in Figure 12. The micrometer positioning device provided a resolution of 0.001 inches in the specification of the radial position of the hot wire sensor. To avoid hitting the probe against the tube wall, radial traverses were begun 0.0035 inches from the wall.

Axial static pressure drop measurements were made. One-eighth inch pressure taps were drilled through the wall of the test facility. The first tap was located 26.6, and the last 52.5, tube diameters from the inlet. The holes were carefully machined, to ensure that they were free of burrs. The pressure lines were fed into a manifold, and pressure differential measurements were made relative to the static pressure tap located 26.6 diameters from the tube inlet. The measurements were made with a Pace-Wianko Model P90D Pressure Transducer together with a Pace Model CD10 Carrier-Demodulator. This equipment produced a 10-volt d-c output signal per inch of water differential pressure. The d-c output was sampled and stored on paper tape, using the data acquisition system. The paper tape was fed into a CDC-160A digital computer, where dimensionless pressure drops were calculated, and where a least squares analysis was performed on the data. A pressure calibration and a check on the linearity of the transducer were made, using a Meriam inclined manometer having a pressure resolution of 0.01 inches of water. The results of the calibration are shown in Figure 29.

4.3.2 Droplet Flow Measurements

Goldschmidt[42] discussed the use of a hot wire anemometer as a droplet sensor. Goldschmidt and Eskenazi[41] used a constant current

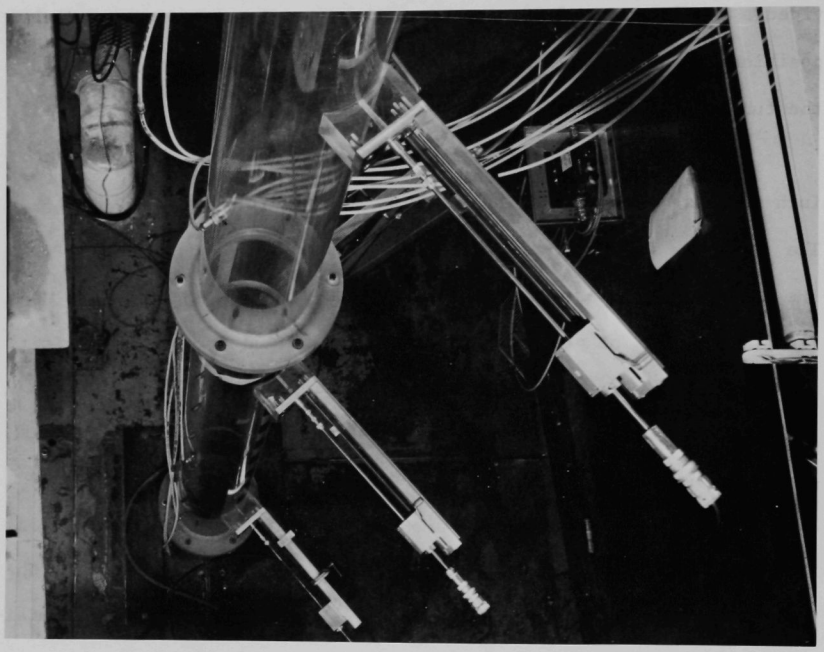

Fig. 12. Radial Traverse Apparatus

anemometer to detect 1-10 micron diameter droplets.

Consider a hot wire probe exposed to a stream of droplets flowing in a turbulent gas. The rate of heat transfer from the hot wire to the fluid is equal to the sum of the contributions from the flow of gas, and from the flow of liquid, past the wire. The fluctuating anemometer voltage signal may be written as the sum of the effects of the turbulent gas and the droplet impactions on the wire, i.e.,

$$e = e_g + e_d \ . \tag{4-2}$$

Application of the hot wire technique to the measurement of droplet flow is expected to be successful if the droplet impaction signal can be discriminated from the turbulent gas signal. The requirement is that

$$e_d >> e_g \ . \tag{4-3}$$

Figure 13 is a schematic of the electronic components employed to detect droplet impactions on the wire. The anemometer output signal was fed into a Tektronix oscilloscope. The oscilloscope was operated as a Schmidt trigger which, when fired, produced a 15-volt ramp-type voltage signal. This signal was picked up at the Gate A output terminal of the oscilloscope. The oscilloscope was also used to visually monitor the anemometer output. The Gate A output pulse was fed into a Computer Measurement Company Model 728AN Universal Counter-Timer, where the droplet impaction pulses were counted.

Several factors determine whether a droplet approaching the hot wire produces a countable pulse:

(a) Impaction misses: If the momentum (per unit volume) of a droplet approaching the hot wire is less than, or nearly equal to, the

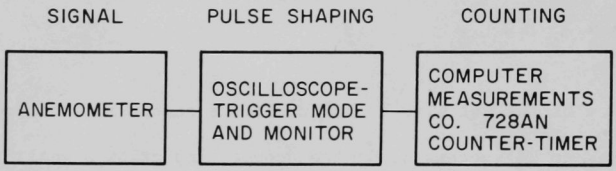

Fig. 13. Electronic Components Used in Droplet Flow Measurements

fluid momentum, it may follow the flow streamlines around the wire and avoid impaction. If the momentum is large, the droplet crosses streamlines and hits the wire. The magnitude of this effect depends on the ratio of droplet diameter to wire diameter. In this research, the ratio was greater than ten. The droplets, therefore, did not escape impaction.[48]

(b) Coincidence impactions: If two or more droplets impact on the wire within a small enough time interval, the impaction pulses of some of the droplets may fall within the dead-time of the counting circuitry. Some droplets, therefore, may not be counted. This effect depends on the droplet concentration level and on the counting circuit dead-time. The maximum impaction rate encountered was approximately 30 sec^{-1}. For this case, a droplet impacted on the wire on the average of once every 30 msec. The oscilloscope sweep time was chosen to be 0.1 msec. No coincidences were observed on the oscilloscope trace.

(c) Signal level: A droplet hitting a wire in a glancing collision is expected to produce a voltage pulse of smaller magnitude than one impacting with a head-on collision. This is expected since the cross sectional area for heat transfer from the wire is smaller for the case of a glancing impaction than for a head-on collision. Small pulses may be lost in the air turbulence signal and may not be counted. The quantity which was measured in this research is C(r,z)/CMAX. The fraction of droplets which were not counted appears as a multiplier in the numerator and in the denominator of this quantity, and hence, cancels out. Quantitative information regarding the magnitude of this effect, therefore, is not required.

Figure 14 is an oscilloscope trace of the anemometer signal show-

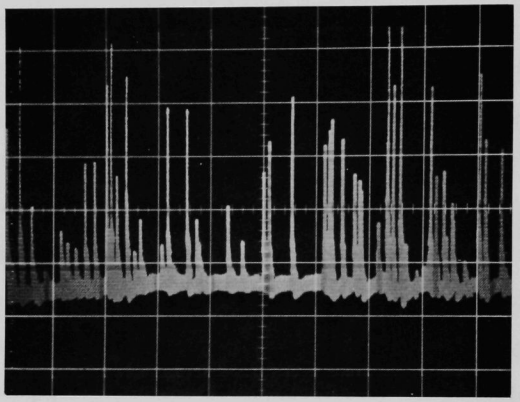

Fig. 14. Anemometer Signal with Droplets Impacting on Sensor

ing the combined effects of turbulence and droplet impactions. The large voltage spikes, representing the droplet impactions, are clearly discernible from the air turbulence signal. Two types of droplet impaction signals are illustrated in Figure 15. The upper oscilloscope trace indicates that a droplet impacted on the wire and immediately detached. The lower trace indicates that after impact, a fragment of liquid remained on the wire until it was either torn from or was boiled from the wire.

In the early stages of the investigation, the anemometer signal was fed directly into the counter. The count rate was compared to the number of pulses observed on oscilloscope traces such as shown in Figure 14. The comparison indicated that more pulses were being counted than actually appeared in the trace. Further investigation revealed that single droplet impaction was causing the anemometer to oscillate, as shown on the trace in Figure 16. A droplet impaction, therefore, resulted in more than a single count. The problem was eliminated by simply turning down the gain of the system until the oscillation disappeared.

The hot wire sensor was used as a droplet concentration probe. This application of the sensor is based on the following considerations: The wire presents a frontal area to the droplet stream equal to the product of the wire diameter and the wire length. The rate of droplet impaction on the wire is proportional to J_z, the number of droplets per unit area per second which strike the wire. For the case of turbulent pipe flow, the axial component of the droplet number flux, J_z, is given by

$$J_z(r,z) = [U(r,z) + u_t]C(r,z), \qquad (4\text{-}4)$$

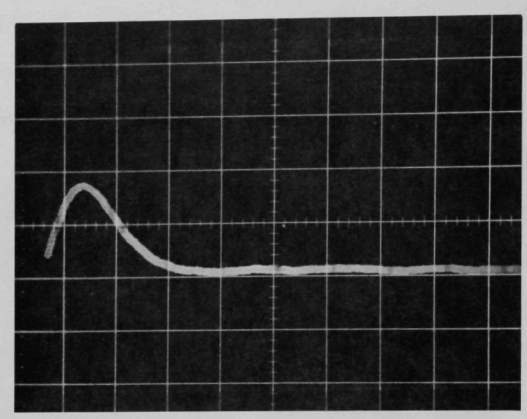

A

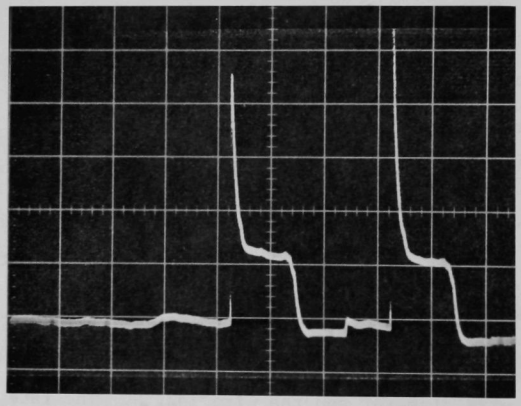

B

Fig. 15. Anemometer Signals with Single Droplet Impaction

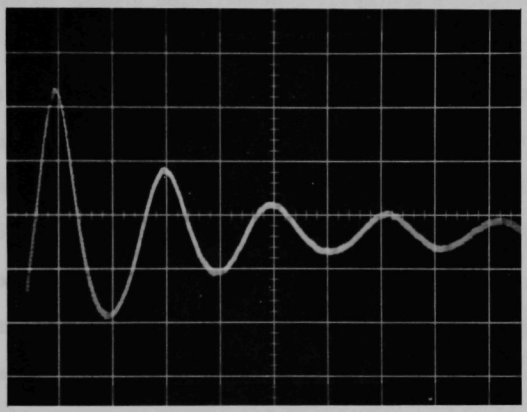

Fig. 16. Anemometer Signal Showing Oscillatory Behavior

where $U + u_t$ is the local mean axial droplet velocity, and $C(r,z)$ is the local droplet concentration. Assume that in the central region of the pipe the droplet velocity $U + u_t$ is spatially independent. For this case, Equation (4-4) implies that the droplet flux is proportional to the droplet concentration. The hot wire sensor, under these circumstances, functions as a droplet concentration probe.

4.3.3 Experience with Additional Experimental Techniques

Attempts were made to use three experimental techniques other than the hot wire anemometer for the measurement of the droplet flow system.

A fiber optic light attenuation probe was developed to sense local droplet concentration. This technique has been employed in studies of solid particle motion to measure particulate concentration and mass flux.[35,58] The work reported here appears to be the first attempt to apply the fiber optic technique to liquid-gas systems. The major difficulty encountered with the first probe that was constructed was the deposition of droplets on the optically polished sensing faces of the fiber bundles. A second probe was constructed to allow passage of a stream of air through the probe in order to blow the collected liquid off the sensing faces of the probe. It was thought that the concentration measurement could be made immediately after a burst of air was sent through the device and before droplet deposition would cause problems. Deposition, however, occurred too fast for the measurement to be made. Because of time considerations, and since the hot wire technique proved successful, work with the fiber optic probe was terminated.

A isokinetic sampling probe[59,60] was designed to be employed as a liquid mass flux detector. The droplet fluxes encountered in the

experiment were too small to make effective use of this technique.

High-speed Fastax motion pictures of the droplets in the flow tube were taken. The objectives of this work were to measure droplet mean velocity, and to assess the value of the technique in the measurement of droplet concentration. Initial results indicated that the technique could be successfully employed to measure droplet velocity. This work was not continued because of time limitations.

4.4 Experimental Procedure

4.4.1 Air Flow Measurements

The air flow measurements were made at Reynolds numbers: 25,000, 50,000, and 100,000. At the beginning of each run, the anemometer probe was inserted into the flow at the center of the pipe. The gate used to control the flow of air was adjusted until the mean anemometer output voltage indicated that the flow was at the desired Reynolds number. Radial traverses of the flow field were made with the hot wire probes at axial positions 17.6, 33.6, 40.0, and 57.2 diameters from the inlet to the flow tube. The relative positions of the axial measuring stations are shown schematically in Figure 17. Mean axial velocity and axial turbulent intensity distributions were obtained in this manner for each Reynolds number and for each axial position.

4.4.2 Droplet Flow Measurements

The droplet flow measurements were made at Reynolds numbers 25,000, 50,000, and 100,000. Three droplet sizes were studied: 80μ, 150μ, and 200μ. Radial traverses of the droplet flow field were made with the hot wire probe at axial positions 6.4, 12.8, 19.2, and 36.3 tube diameters from the droplet injector. At each of these axial positions, shown schematically in Figure 17, the radial distribution of drop-

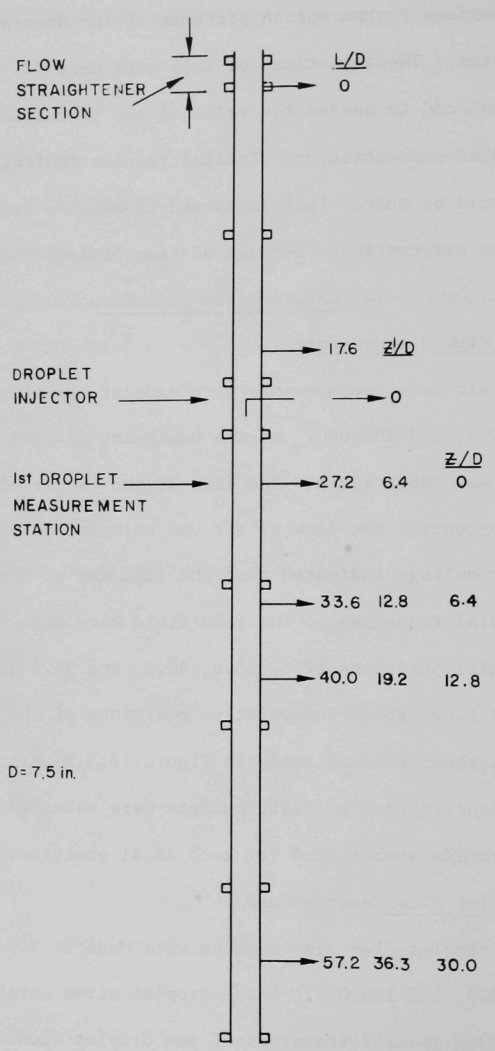

Fig. 17. Hot Wire Probe Measurement Stations

let impaction rate was measured. The rate of droplet impaction on the hot wire sensor was proportional to the droplet concentration. The radial traverses, therefore, resulted in measurement of the droplet concentration distributions.

At the beginning of each droplet flow experimental run, the air flow rate was adjusted to obtain the proper Reynolds number. A liquid injector nozzle, chosen to produce droplets with the desired diameter, was inserted into the droplet injector assembly. The gas bottle pressure regulator was adjusted to supply the system pressure necessary to give the desired liquid flow rate. The oscillator was set at the frequency required for the production of droplets with the desired diameter. The frequency was calculated using Equation (4-1).

V. EXPERIMENTAL RESULTS

5.1 Air Flow Measurements

5.1.1 Mean Axial Velocity

Local mean axial velocity measurements were made with the hot wire anemometer at Reynolds numbers 25,000, 50,000, and 100,000, and at axial positions 17.6, 33.6, 40.0, and 57.2 tube diameters from the inlet to the flow tube. The measurements were carried out with and without the droplet injector section present in the duct. The results of these measurements are presented in Figure 18 to 23.

The first series of measurements were made without the liquid injector section present in the flow tube. Figure 18 shows that the reproducibility of the measurements was generally within $\pm 3\%$. Figure 18 also reveals asymmetries in the velocity distributions measured 33.6 and 40.0 diameters from the tube inlet. The maximum velocity is shifted by 0.1R off the axis of the tube. The slope of the velocity profile to the right of r/R=0 is greater than that of the other side. The measurement was repeated with the flow tube holding the probe rotated 180°. Figure 19 is a composite of the two measurements, and represents a complete traverse of the tube diameter. The asymmetry is less marked, although still observable. The reason for the asymmetry was not definitely established. The asymmetry may have been caused, however, by nonuniformities in one or more of the Lucite flow tubes.

Figure 20 is a comparison of the mean velocity profile measured here with that measured by Laufer,[50] for Re = 50,000. For half duct diameter the agreement is within 3%. The relatively poor agreement for

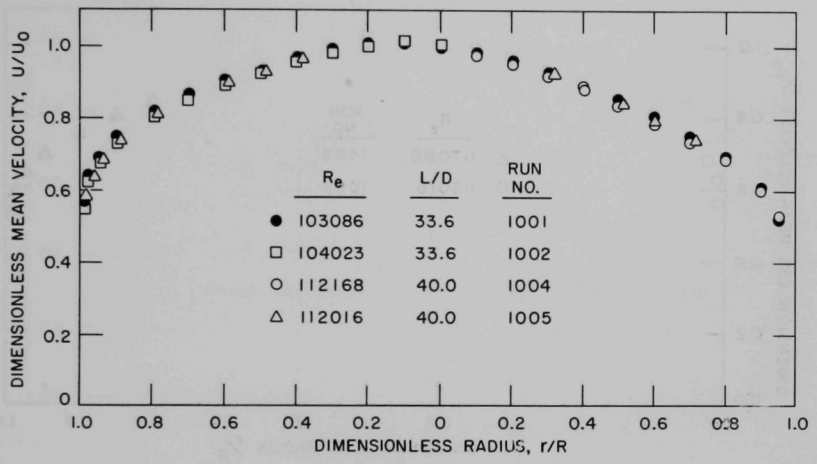

Fig. 18. Reproducibility of Mean Velocity Distribution Data

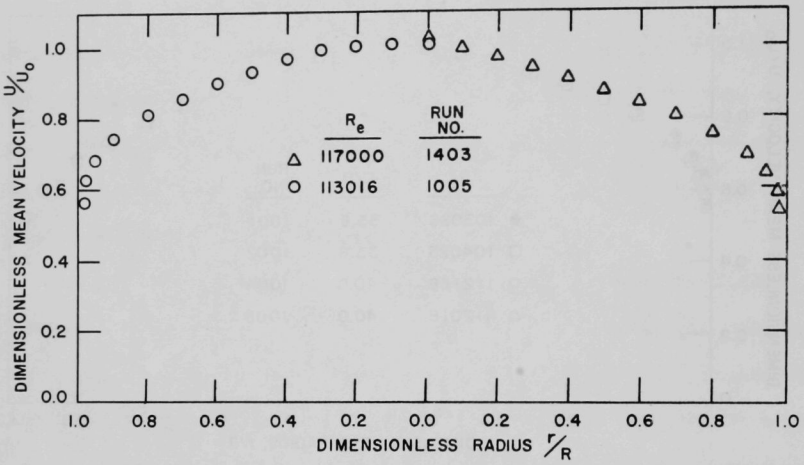

Fig. 19. Mean Velocity Distribution: Composite of Two Traverses Made 180° Apart

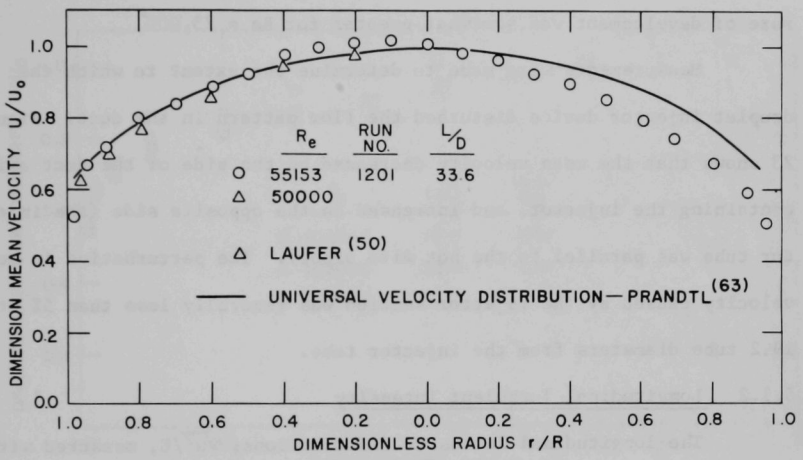

Fig. 20. Comparison of Mean Velocity Distributions with Published Data

the other half of the duct diameter is apparently the result of the asymmetry discussed above.

The development of the mean velocity profile is shown in Figures 21 and 22. For Re = 100,000, the mean velocity profile was nearly fully developed 30 tube diameters from the entrance to the flow tube. The rate of development was somewhat greater for Re = 25,000.

Measurements were made to determine the extent to which the droplet injector device disturbed the flow pattern in the duct. Figure 23 shows that the mean velocity decreased on the side of the duct axis containing the injector, and increased on the opposite side (the injector tube was parallel to the hot wire probe). The perturbation in mean velocity caused by the injector section was generally less than 5% at 19.2 tube diameters from the injector tube.

5.1.2 Longitudinal Turbulent Intensity

The longitudinal intensity distributions, $\sqrt{u^2}/U$, measured with the hot wire anemometer, are presented in Figures 24 to 27. The results show that the turbulent intensity distributions were asymmetric. The reasons for the asymmetry are discussed in the previous section. Figure 24 shows that the reproducibility of the intensity measurement was within $\pm 3\%$.

The development of the longitudinal intensity profiles is shown in Figures 25 and 26. The intensity distributions were nearly fully developed 40 tube diameters from the inlet to the duct.

The effect of the injector tube section on the intensity profiles is shown in Figure 27. Apparently, the effect of the injector section was to enhance the asymmetry in the profiles.

Figure 28 compares the longitudinal turbulent velocity profiles

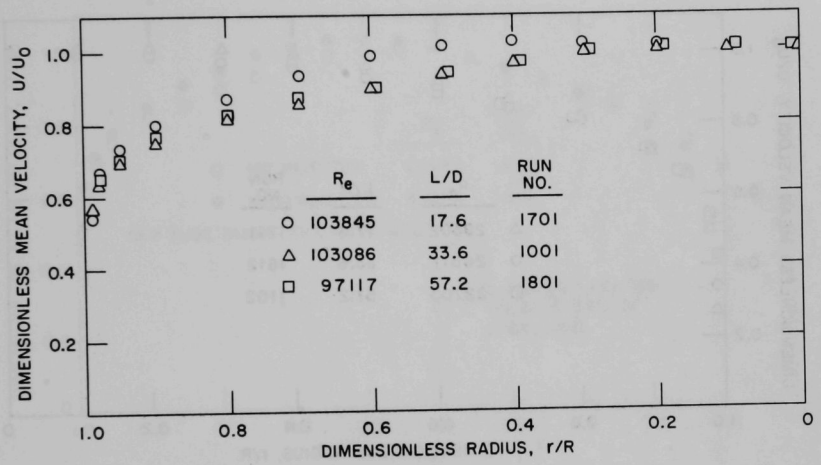

Fig. 21. Development of Mean Velocity Distributions: Re = 100,000

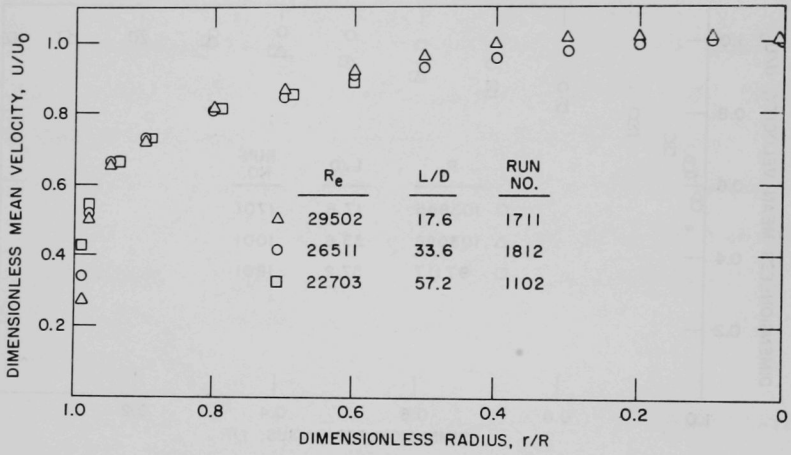

Fig. 22. Development of Mean Velocity Distributions: Re = 25,000

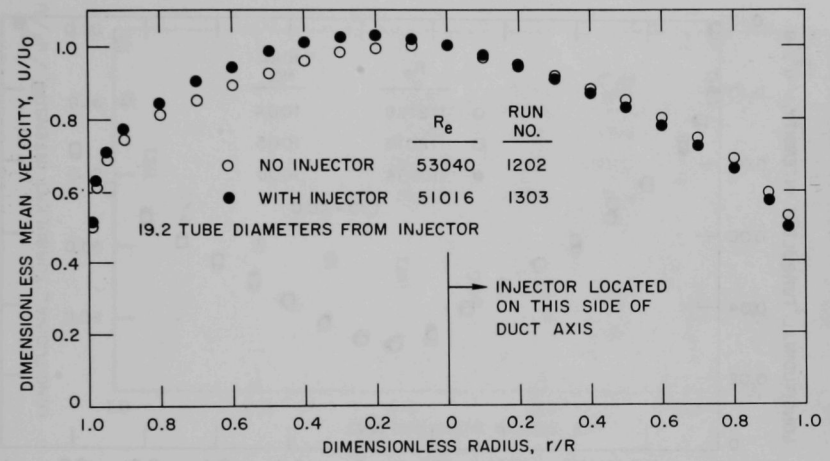

Fig. 23. Effect of Injector Assembly on Mean Velocity Distributions

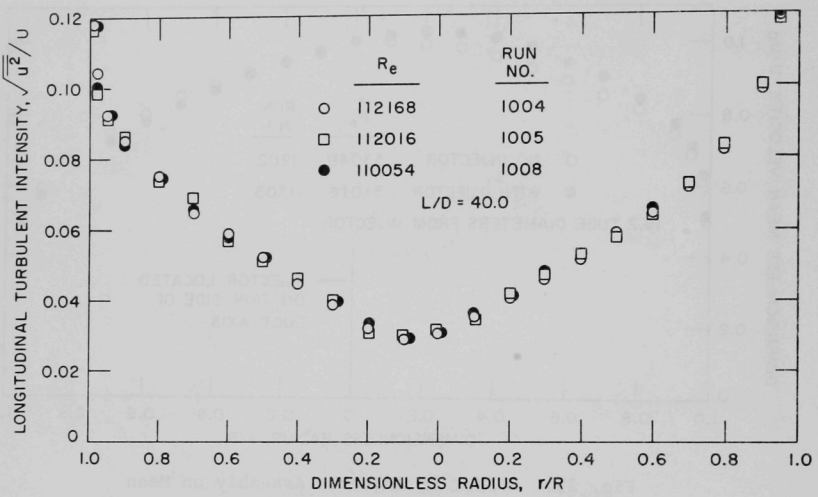

Fig. 24. Reproducibility of Turbulent Intensity Distribution Data

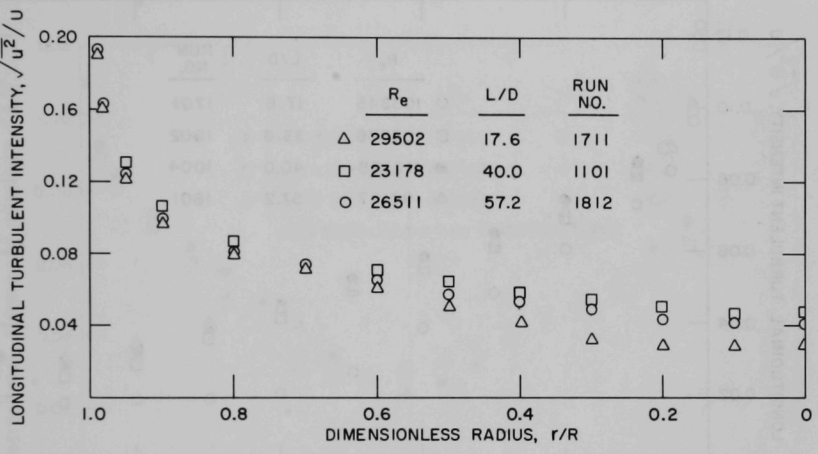

Fig. 25. Development of Turbulent Intensity Distributions: Re = 25,000

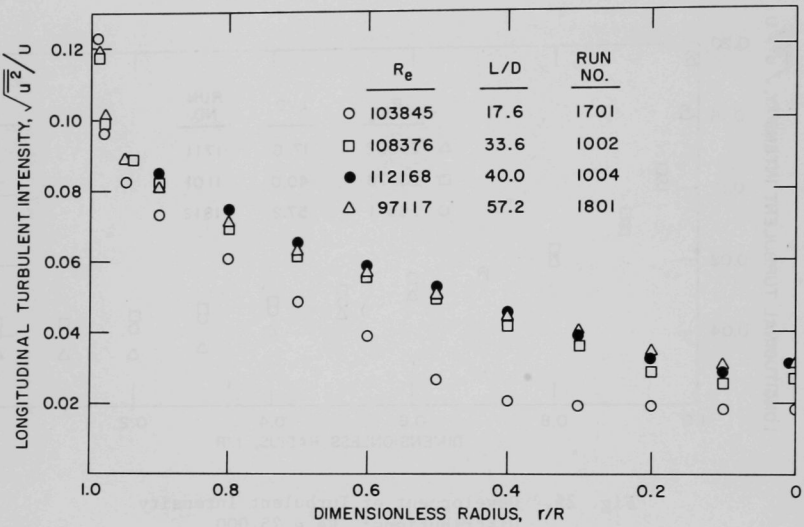

Fig. 26. Development of Turbulent Intensity Distributions: Re = 100,000

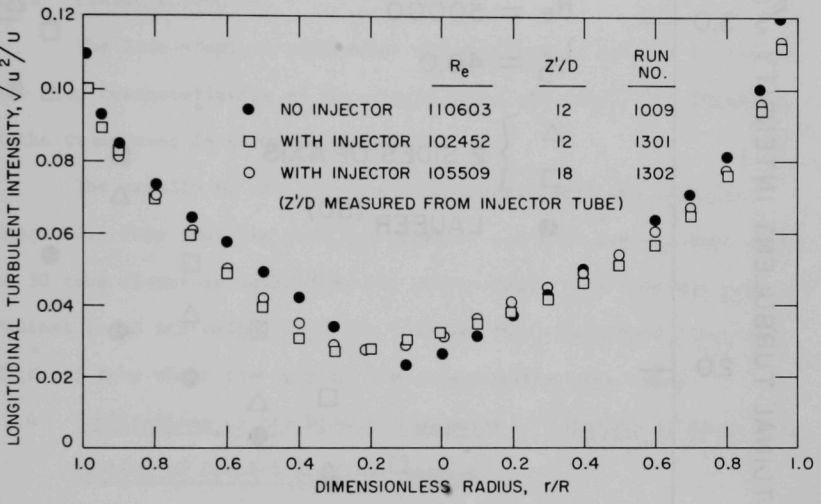

Fig. 27. Effect of Injector Assembly on Turbulent Intensity Distributions

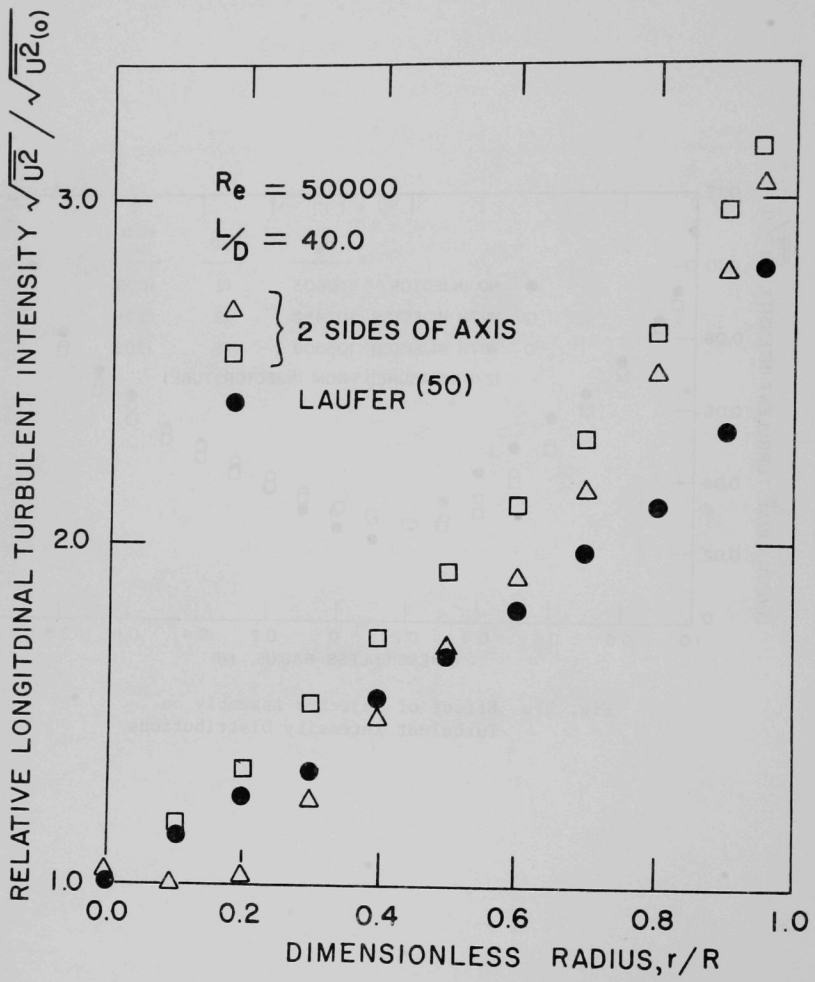

Fig. 28. Comparison of Turbulent Intensity Distributions with Published Data

with Laufer's data, for Re = 50,000. Although the results agree qualitatively, there are considerable quantitative differences. The reasons for the discrepancies have not been established.

The centerline (r/R=0) turbulent intensities agree favorably with those determined by other authors.[52]

5.1.3 Pressure Drop

The Pace pressure transducer was employed to measure the pressure drop characteristics of the single phase air flow. The linearity of the transducer is shown in Figure 29.

The results of the pressure drop measurements are shown in Figure 30. They indicate that the pressure gradient was constant over the 30 tube diameters covered by the static taps. The constant pressure gradient is an indication that the flow was fully developed along the length of tube where the droplet flow measurements were made.

5.1.4 Implications of Air Flow Measurements in Relation to Axial Positioning of Droplet Injector Section

The air flow measurements indicate that the mean velocity profiles were nearly fully developed approximately 30 tube diameters from the inlet to the flow tube. The longitudinal intensity profiles were nearly fully developed 40 diameters from the tube inlet. The results also indicate that the static pressure gradient was constant for $L/D > 27$.

In the droplet-flow experiments, the droplet injector was placed in the flow tube at an axial position 20 tube diameters from the inlet. The first droplet-flux measurements were made at a position 27 diameters from the inlet. The turbulent intensity distributions were not yet fully developed at this position. This arrangement was chosen, however, to al-

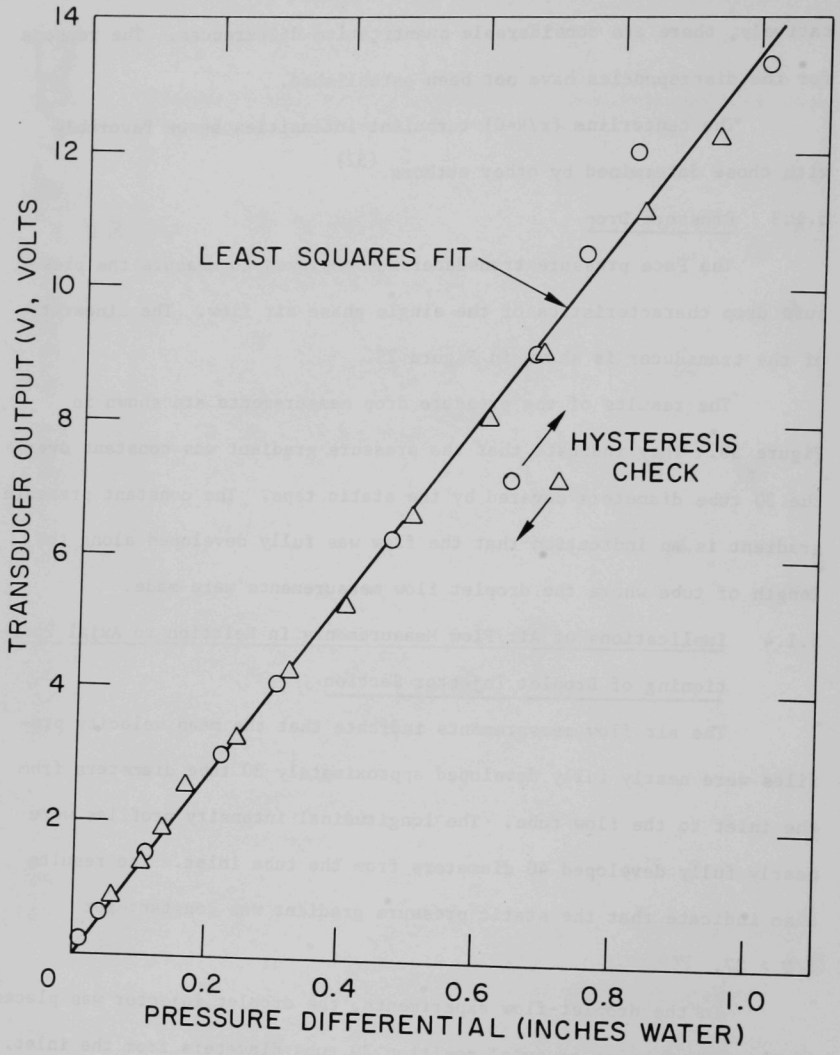

Fig. 29. Pressure Transducer Calibration Curve

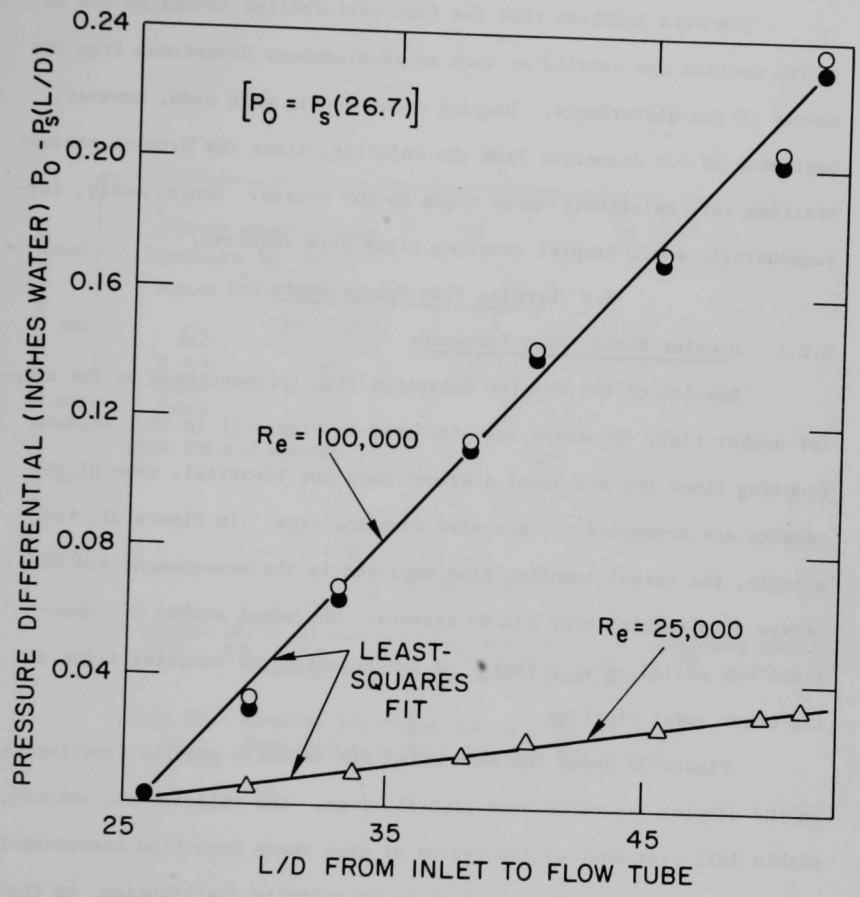

Fig. 30. Differential Static Pressure Measurements

low a large axial distance downstream from the source in which to carry out the droplet flow experiments.

The data indicate that the flow perturbation caused by the injector section was carried as much as 18 diameters downstream from the source of the disturbance. Droplet measurements were made, however, beginning at 6.4 diameters from the injector, since the droplet concentrations were relatively large close to the source. Consequently, correspondingly small droplet counting times were required.

5.2 Droplet Flow Measurements

5.2.1 Droplet Number Flux Traverses

Results of the droplet impaction rate (proportional to the droplet number flux) traverses are presented in Figure 31 to 33. Because counting times for all axial stations were not identical, some of the results are presented for a scaled counting time. In Figure 31, for example, the actual counting time employed in the measurement 6.4 diameters from the injector was 90 seconds. The total number of impactions was scaled up by a factor of two to match the counting times at the other axial stations.

Figure 32 shows the mean axial air velocity profile superimposed on the droplet impaction rate distributions. The velocity was uniform, within 10%, over most of the region of pipe where impaction measurements were made. The lack of nonuniformity in velocity distribution, on the right side of Figure 32, is accounted for by the asymmetry in the axial velocity distribution discussed in a previous section. The effect of the asymmetry on the results is discussed in Section 5.2.3.

The statistical scatter of the impaction rate data is illustrated in Figure 31 and 33. For the 200μ droplets, the impaction rates were

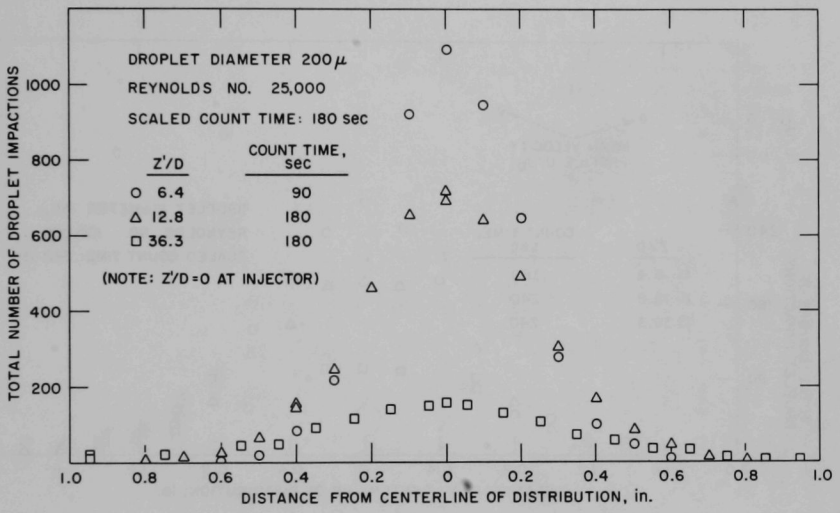

Fig. 31. Droplet Impaction Rate Distributions with Mean Velocity Distribution Superposed

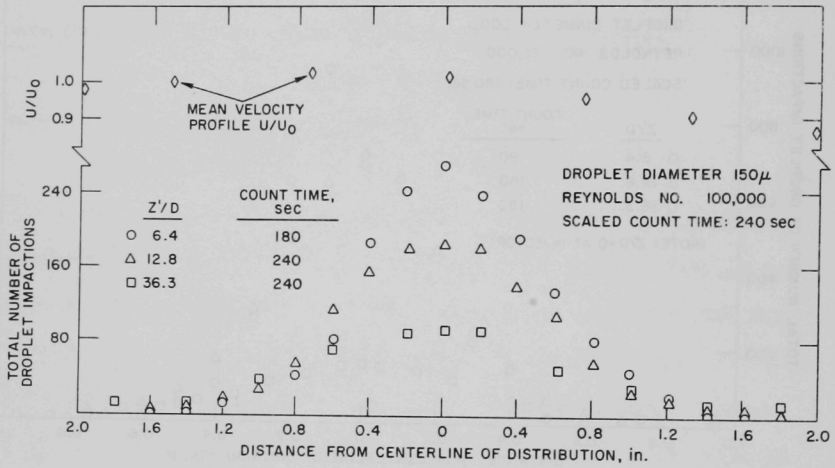

Fig. 32. Droplet Impaction Rate Distributions

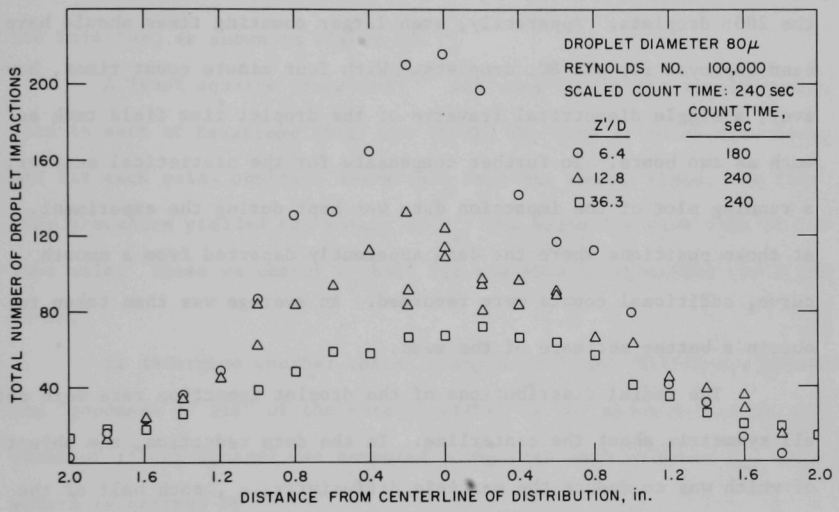

Fig. 33. Droplet Impaction Rate Distributions

significantly greater than for the 80 μ drops. Larger counting times were, therefore, employed in gathering the 80 μ data, and also in obtaining data 36 tube diameters from the injector. Even with this compensation, the scatter in the 80 μ data was such that deviations of 25% from the mean in total impactions at the centerline (r/R = 0) were not uncommon. This compares with deviations of 5-10% at the centerline for the 200 μ droplets. Apparently, even larger counting times should have been employed for the 80 μ droplets. With four minute count times, however, a single diametrical traverse of the droplet flow field took as much as two hours. To further compensate for the statistical scatter, a running plot of the impaction data was kept during the experiment. At those positions where the data apparently departed from a smooth curve, additional counts were recorded. An average was then taken to obtain a better estimate of the mean.

The radial distributions of the droplet impaction rate were not all symmetric about the centerline. In the data reduction, the object of which was to deduce the particle diffusivity, ε_p, each half of the radial traverse was analyzed separately. At each measurement station downstream from the source plane, therefore, two radial distributions were obtained. Two values of ε_p were deduced: one for each radial distribution. If the droplet flux distributions had been symmetric, the two values of ε_p would be identical. This is not generally the case, as discussed in Section 5.2.3.

5.2.2 Data Reduction Technique

The droplet impaction rate was proportional to the number flux, and hence to the droplet concentration. The droplet impaction data, for each set of droplet and air flow parameters, were fitted to the equations

$$C(r,z) = CMAX\phi_1(r,z) \qquad (5\text{-}1)$$

$$C(r,z) = CMAX\phi_2(r,z'), \qquad (5\text{-}2)$$

where ϕ_1 and ϕ_2 are the plane and point source solutions, respectively, to the one-dimensional diffusion equation, defined in Section 3.1.4. The axial distance z is measured from the source plane, and z' from the injector, as shown in Figure 17.

A least squares procedure[49] was used to fit the concentration data to each of Equations (5-1) and (5-2). For each of these equations, and for each axial position downstream from the source plane, the fitting procedure yielded two values of ε_p: one value for each side of the tube axis. These values of ε_p best fit the data to Equations (5-1) and (5-2).

To determine whether there is any significant difference between the "goodness of fit" of the data to either of the above equations, a value of χ^2(chi-square) was computed along with each value of ε_p. Chi-square is defined by

$$\chi^2 = \sum_i \frac{[C(\text{observed})_i - C(\text{calculated})_i]^2}{C(\text{observed})_i} . \qquad (5\text{-}3)$$

The results of these computations are presented and discussed in the next section.

5.2.3 Particle Diffusivity Results and Analysis

Tables 1 to 3 present the particle diffusivity data extracted from the droplet concentration distributions. The quantities $\varepsilon_p(1)$ and $\varepsilon_p(2)$ are the diffusivities obtained for the two halves of the complete diametrical traverse of the flow distribution. They were deduced from

TABLE 1 – Results of Least Squares Analysis of Droplet Concentration Data: d = 200μ

		PLANE SOURCE				POINT SOURCE			
Re	z	$\varepsilon_p(1)$	χ_1^2	$\varepsilon_p(2)$	χ_2^2	$\varepsilon_p(1)$	χ_1^2	$\varepsilon_p(2)$	χ_2^2
25,000	4	0.000195	24.3	0.000242	7.0	0.000182	25.2	0.000214	8.2
	8	0.000152	5.5	0.000252	15.4	0.000158	5.5	0.000231	15.1
	19	0.000157	18.7	0.000143	12.3	0.000159	18.2	0.000151	12.3
	4	0.000118	33.6	0.000242	8.1	0.000144	34.6	0.000214	8.9
		$\overline{\varepsilon_p(1)} = 0.000155 \pm 0.000027$				$\overline{\varepsilon_p(1)} = 0.000161 \pm 0.000014$			
		$\overline{\varepsilon_p(2)} = 0.000219 \pm 0.000044$				$\overline{\varepsilon_p(2)} = 0.000203 \pm 0.000031$			
		$\varepsilon_p = 0.000182 \pm 0.000032$				$\varepsilon_p = 0.000187 \pm 0.000490$			
50,000	4	0.000375	112.0	0.000243	22.3	0.000432	127.0	0.000305	23.1
	8	0.000352	8.9	0.000366	20.6	0.000396	10.4	0.000363	21.8
	19	0.000412	31.0	0.000376	19.5	0.000429	31.5	0.000374	19.7
		$\overline{\varepsilon_p(1)} = 0.000380 \pm 0.000025$				$\overline{\varepsilon_p(1)} = 0.000419 \pm 0.000016$			
		$\overline{\varepsilon_p(2)} = 0.000328 \pm 0.000061$				$\overline{\varepsilon_p(2)} = 0.000347 \pm 0.000030$			
		$\varepsilon_p = 0.000354 \pm 0.000053$				$\varepsilon_p = 0.000383 \pm 0.000043$			

TABLE 1 – Results of Least Squares Analysis of Droplet Concentration Data: d=200μ(cont.)

		PLANE SOURCE				POINT SOURCE			
Re	z	$\varepsilon_p(1)$	χ_1^2	$\varepsilon_p(2)$	χ_2^2	$\varepsilon_p(1)$	χ_1^2	$\varepsilon_p(2)$	χ_2^2
100,000	4	0.00107	51.0	0.00161	19.8	0.00103	54.2	0.00124	19.7
	8	0.00119	27.2	0.00156	13.2	0.00124	27.8	0.00133	13.1
	19	0.00096	18.3	0.00105	23.7	0.00097	18.2	0.00103	23.7

$\overline{\varepsilon_p(1)} = 0.00107 \pm 0.00009$

$\overline{\varepsilon_p(2)} = 0.00141 \pm 0.00025$

$\varepsilon_p = 0.00124 \pm 0.00025$

$\overline{\varepsilon_p(1)} = 0.00108 \pm 0.00012$

$\overline{\varepsilon_p(2)} = 0.00120 \pm 0.00013$

$\varepsilon_p = 0.00114 \pm 0.00013$

TABLE 2 – Results of Least Squares Analysis of Droplet Concentration Data: d = 150μ

		PLANE SOURCE				POINT SOURCE			
Re	z	$\varepsilon_p(1)$	χ_1^2	$\varepsilon_p(2)$	χ_2^2	$\varepsilon_p(1)$	χ_1^2	$\varepsilon_p(2)$	χ_2^2
25,000	4	0.000378	6.6	0.000322	16.0	0.000275	5.5	0.000255	16.8
	8	0.000226	2.5	0.000188	3.1	0.000209	2.7	0.000189	3.2
	19	0.000331	5.9	0.000244	34.0	0.000305	5.9	0.000236	33.6
		$\overline{\varepsilon_p(1)} = 0.000312 \pm 0.000064$				$\overline{\varepsilon_p(1)} = 0.000263 \pm 0.000040$			
		$\overline{\varepsilon_p(2)} = 0.000251 \pm 0.000055$				$\overline{\varepsilon_p(2)} = 0.000227 \pm 0.000028$			
		$\varepsilon_p = 0.000282 \pm 0.000067$				$\varepsilon_p = 0.000245 \pm 0.000039$			
50,000	4	0.00129	11.8	0.00157	11.7	0.00172	6.2	0.000968	11.4
	8	0.00104	10.8	0.00130	4.5	0.00145	7.3	0.000756	3.7
	19	0.00106	8.5	0.00095	17.2	0.00132	8.7	0.000633	17.2
		$\overline{\varepsilon_p(1)} = 0.00113 \pm 0.000160$				$\overline{\varepsilon_p(1)} = 0.00150 \pm 0.000177$			
		$\overline{\varepsilon_p(2)} = 0.00127 \pm 0.000138$				$\overline{\varepsilon_p(2)} = 0.00139 \pm 0.00013$			
		$\varepsilon_p = 0.00120 \pm 0.000214$				$\varepsilon_p = 0.00144 \pm 0.00016$			

TABLE 2 - Results of Least Squares Analysis of Droplet Concentration Data: d = 150μ (cont.)

		PLANE SOURCE				POINT SOURCE			
Re	z	$\varepsilon_p(1)$	χ_1^2	$\varepsilon_p(2)$	χ_2^2	$\varepsilon_p(1)$	χ_1^2	$\varepsilon_p(2)$	χ_2^2
100,000	4	0.00890	2.2	0.00740	6.4	0.00682	2.3	0.01060	6.3
	8	0.00467	3.5	0.00490	3.9	0.00473	3.5	0.00520	3.9
	19	0.00346	6.6	0.00705	5.1	0.00372	6.6	0.00765	5.1
		$\overline{\varepsilon_p(1)} = 0.00568 \pm 0.00233$				$\overline{\varepsilon_p(1)} = 0.00509 \pm 0.00172$			
		$\overline{\varepsilon_p(2)} = 0.00782 \pm 0.00221$				$\overline{\varepsilon_p(2)} = 0.00645 \pm 0.00111$			
		$\varepsilon_p = 0.00675 \pm 0.00251$				$\varepsilon_p = 0.00577 \pm 0.00181$			

TABLE 3 - Results of Least Squares Analysis of Droplet Concentration Data: d = 80μ

		PLANE SOURCE				POINT SOURCE			
Re	z	$\varepsilon_p(1)$	χ_1^2	$\varepsilon_p(2)$	χ_2^2	$\varepsilon_p(1)$	χ_1^2	$\varepsilon_p(2)$	χ_2^2
25,000	4	0.000284	12.5	———	———	0.000293	12.6	0.000268	14.4
	19	0.000440	7.2	———	———	0.000417	7.2	0.000392	7.5
		$\overline{\varepsilon_p(1)} = 0.000362 \pm 0.000078$				$\overline{\varepsilon_p(1)} = 0.000355 \pm 0.000062$			
		$\varepsilon_p = 0.000294 \pm 0.000078$				$\overline{\varepsilon_p(2)} = 0.000330 \pm 0.000062$			
						$\varepsilon_p = 0.000343 \pm 0.000015$			
25,000	4	0.000208	10.2	———	———	0.000290	9.9	0.000248	23.7
	19	0.000244	29.5	———	———	0.000271	30.1	0.000268	30.0
		$\overline{\varepsilon_p(1)} = 0.000226 \pm 0.000018$				$\overline{\varepsilon_p(1)} = 0.000281 \pm 0.000095$			
		$\varepsilon_p = 0.000294 \pm 0.000088$				$\overline{\varepsilon_p(2)} = 0.000258 \pm 0.000010$			
						$\varepsilon_p = 0.000306 \pm 0.000059$			

TABLE 3 - Results of Least Squares Analysis of Droplet Concentration Data: d = 80μ (cont.)

		PLANE SOURCE				POINT SOURCE			
Re	z	$\varepsilon_p(1)$	χ_1^2	$\varepsilon_p(2)$	χ_2^2	$\varepsilon_p(1)$	χ_1^2	$\varepsilon_p(2)$	χ_2^2
50,000	4	0.00128	2.6	0.00141	7.8	0.00135	2.3	0.00146	8.2
	19	0.00193	15.1	0.00097	15.1	0.00111	15.2	0.00107	15.2
		$\overline{\varepsilon_p(1)} = 0.00116 \pm 0.00012$				$\overline{\varepsilon_p(1)} = 0.00123 \pm 0.00012$			
		$\overline{\varepsilon_p(2)} = 0.00119 \pm 0.00022$				$\overline{\varepsilon_p(2)} = 0.00127 \pm 0.00020$			
		$\varepsilon_p = 0.00117 \pm 0.00018$				$\varepsilon_p = 0.00125 \pm 0.00016$			
100,000	4	0.0100	10.1	0.0134	4.6	0.00841	9.9	0.00962	4.6
	19*	0.0029	15.4	0.0036	7.7	0.00368	15.3	0.00403	7.7
	4	0.0108	8.1	0.0143	5.4	0.00897	8.3	0.01070	5.5
	19*	0.0022	11.4	0.0034	33.0	0.00299	11.2	0.00407	32.2
		$\overline{\varepsilon_p(1)} = 0.0104 \pm 0.00028$				$\overline{\varepsilon_p(1)} = 0.00869 \pm 0.000378$			
		$\overline{\varepsilon_p(2)} = 0.0138 \pm 0.00030$				$\overline{\varepsilon_p(2)} = 0.01015 \pm 0.000648$			
		$\varepsilon_p = 0.0121 \pm 0.00052$				$\varepsilon_p = 0.00942 \pm 0.00171$			

* This data not considered. See Section 5.2.4.

the least squares fit to the point and plane source solutions to the diffusion equation. A value of χ^2 is shown for each case. For each droplet size and Reynolds number, the values of $\varepsilon_p(1)$ and $\varepsilon_p(2)$ were arithmetically averaged. These averages are presented as $\overline{\varepsilon_p(1)}$ and $\overline{\varepsilon_p(2)}$. The quantity ε_p is the lumped average diffusivity obtained for each droplet size and Reynolds number.

One object of this study was to test the validity of the turbulent diffusion model, as applied to droplet transport in fully developed turbulent pipe flow. One implication of Taylor's statistical analysis, as applied to particle diffusion, is that the particle diffusivity is independent of distance downstream from a source of droplets. The diffusivities extracted from the data should, therefore, be independent of axial distance from the source. Variation in diffusivity from one axial position to another, of generally less than 30% is apparent in Tables to 3. For the case d = 100μ and Re = 100,000, the variation of ε_p with z is quite marked. For reasons that are discussed in Section 5.2.4 the diffusivity data taken at z = 19 ft were discarded. Generally, however, the results reveal no consistent behavior of ε_p with axial distance. The diffusivities are constant with axial distance to within approximately 30%.

The data labeled $\varepsilon_p(1)$ and $\varepsilon_p(2)$ in Tables 1 to 3 are the diffusivities extracted from the droplet flux traverses for the two sides of the flux distribution centerline. The data are presented in this manner because it was expected that the asymmetries in the mean velocity and turbulent intensity distributions across the tube diameter should reflect similar asymmetries in the droplet concentration distributions. As a consequence, it was expected that the diffusivity data should also

reflect this asymmetry. The data reveal no such trend. Within the accuracy of the experiment, the asymmetry in the air-flow distribution is not reflected in a corresponding asymmetry in the droplet diffusivity results.

Although the diffusivity data do not reveal asymmetries correlating with the air-flow asymmetries, the values of $\overline{\varepsilon_{p(1)}}$ and $\overline{\varepsilon_{p(2)}}$ differ by as much as 35-40% for some of the data sets. This indicates that asymmetries in the droplet flow field were actually present. These asymmetries may have been caused by misalignment of the droplet injector relative to the axis of the flow tube. Although care was taken to align the centerline of the droplet distribution with the tube axis before each experimental run, this was apparently not entirely successful.

The values of ε_p presented in Tables 1 to 3 were obtained as a result of fitting the droplet concentration data to the point and plane source solutions of the diffusion equation. It was expected that the point source solution might not be accurate, since near the source the droplets were accelerating to their steady-state velocity. In addition, close to the source the injector perturbation was expected to be relatively large. At 6.4 tube diameters downstream from the injector, therefore, a plane source distribution was measured. At this position, the droplets had reached their steady-state velocities. This measured source distribution was used with Equation (3-8a) in the least-squares fit to the droplet concentration data. The results indicate no significant differences in the values of ε_p deduced from the least-squares analysis of the data to Equations (3-8a) and (3-8b). In addition, the values of

χ^2 calculated for each case, which represent a measure of the "goodness of fit" of the data to the theoretical model, reveal that the two curves fit the data with nearly the same accuracy. The effects of the mismatch of droplet and air velocities at the droplet injector, and the injector perturbation, are either masked out by experimental uncertainties, or are reflected equally in the ε_p calculated using the two solutions of the diffusion equation.

Figure 34 summarizes the diffusivity data. The particle diffusivity decreases with increasing terminal velocity (or particle response time). This supports the intuitive notion that heavy particles diffuse less readily than light ones. The diffusivity increases with Reynolds number, as the rms turbulent velocity increases.

The quantity $\varepsilon_p/\varepsilon_f$ is the ratio of the particle diffusivity to the turbulent mass diffusivity for molecular size species. It is a measure of the effectiveness of the turbulence in diffusing objects with negligible inertia, as compared to its effectiveness in diffusing relatively heavy particles. If $\varepsilon_p/\varepsilon_f = 1$, then heavy particles are transported by the turbulence with the same effectiveness as molecular size species, and the inertial properties of the particles have negligible influence on the turbulent diffusion process.

The diffusivity ε_f was not determined in these experiments. The quantity could be determined in the same manner as described here for measuring ε_p, by replacing the source of droplets with a source of tracer gas, and measuring the gas concentration downstream from the source. The data in Table 4 were obtained from this type of experiment.[19]

Figure 35 shows the quantity $\varepsilon_p/\varepsilon_f$ plotted against the mean flow Reynolds number. This ratio is roughly one for the 80μ droplets

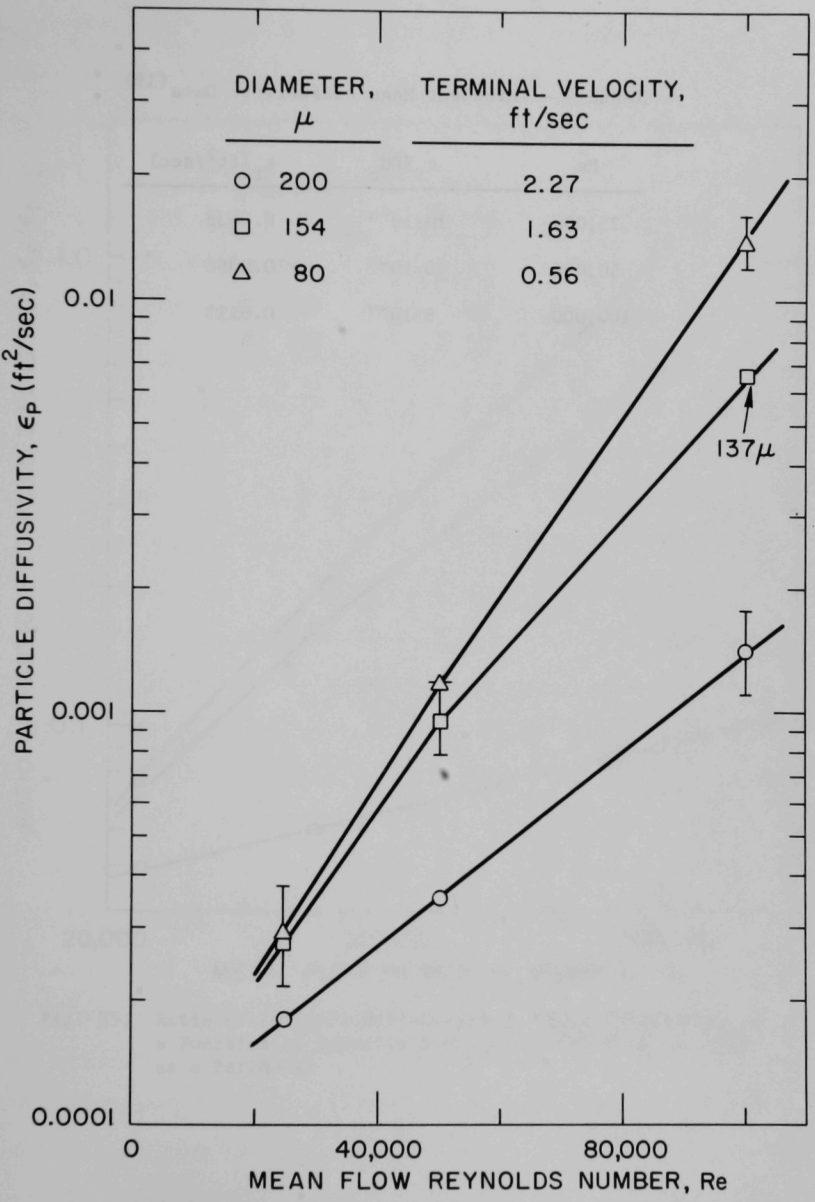

Fig. 34. Particle Diffusivity Data as a Function of Droplet Parameters and Reynolds Number

TABLE 4 - Turbulent Mass Diffusivity Data[19]

Re	ε_f/DU_o	ε_f (ft^2/sec)
25,000	10×10^{-4}	0.0038
50,000	8×10^{-4}	0.0060
100,000	8×10^{-4}	0.0113

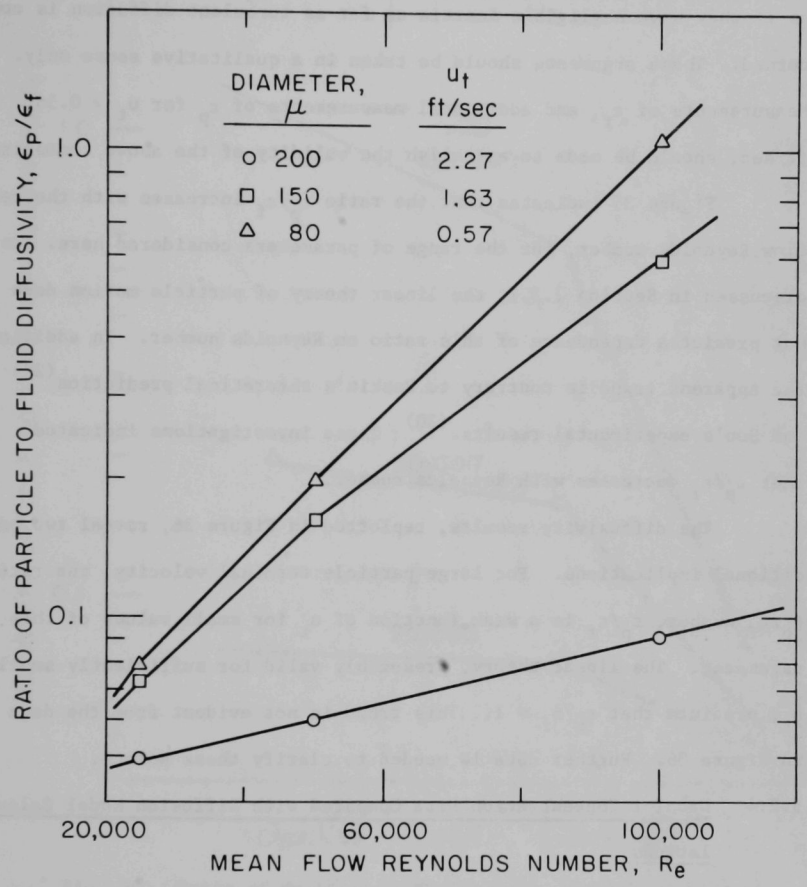

Fig. 35. Ratio of Particle Diffusivity to Fluid Diffusivity as a Function of Reynolds Number with Terminal Velocity as a Parameter

(u_t = 0.56 ft/sec) and for Re = 100,000. This implies that when Re = 100,000, particles with terminal velocity less than 0.56 ft/sec behave as if they have negligible inertia as far as turbulent diffusion is concerned. These arguments should be taken in a qualitative sense only. Measurements of ε_f, and additional measurements of ε_p for $u_t < 0.56$ ft/sec, should be made to establish the validity of the above comments.

Figure 35 indicates that the ratio $\varepsilon_p/\varepsilon_f$ increases with the mean flow Reynolds number, for the range of parameters considered here. As discussed in Section 2.3.1, the linear theory of particle motion does not predict a dependence of this ratio on Reynolds number. In addition, the apparent trend is contrary to Peskin's theoretical prediction[29] and Soo's experimental results.[30] These investigations indicated that $\varepsilon_p/\varepsilon_f$ decreases with Reynolds number.

The diffusivity results, replotted in Figure 36, reveal two additional implications. For large particle terminal velocity, the ratio $\varepsilon_p/\varepsilon_f$ number, $\varepsilon_p/\varepsilon_f$ is a weak function of u_t for small values of this parameter. The linear theory, presumably valid for sufficiently small u_t, predicts that $\varepsilon_p/\varepsilon_f = 1$. This trend is not evident from the data in Figure 36. Further data is needed to clarify these points.

5.2.4 Droplet Concentration Data Compared with Diffusion Model Calculations

In Section 3.1.3, the diffusion model is proposed to describe the transport of droplets in the central core region of turbulent pipe flow. The diffusivity results presented in Figure 34 were used to calculate the concentration distributions downstream from the source plane. This calculation differs from that described in Section 5.2.2, in that a single value of ε_p was employed to calculate the droplet concentration

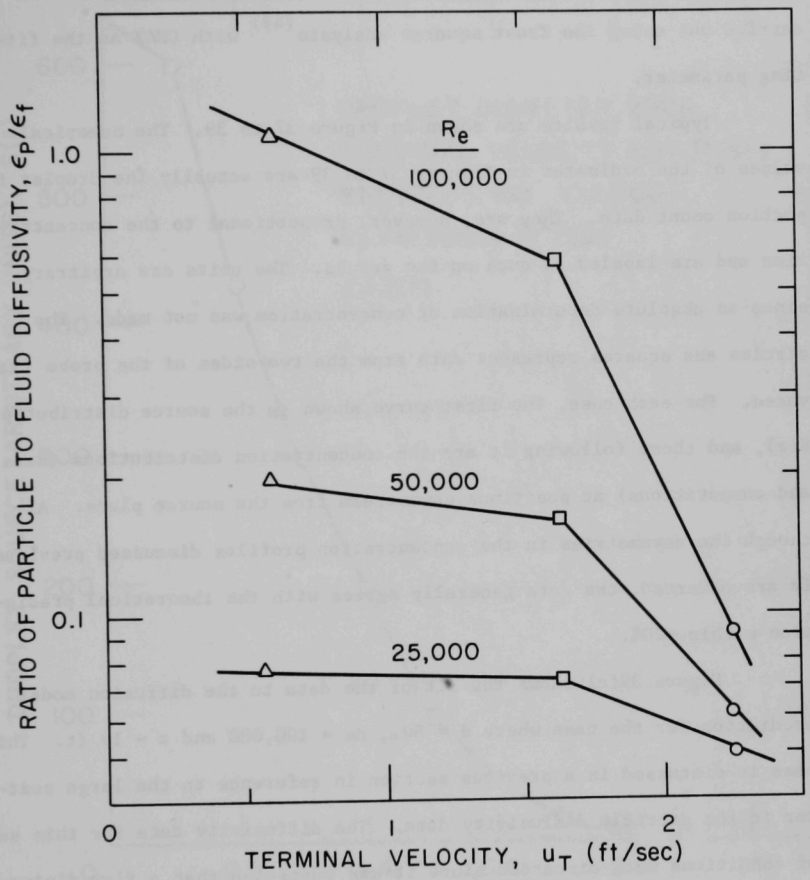

Fig. 36. Ratio of Particle Diffusivity to Fluid Diffusivity as a Function of Terminal Velocity with Reynolds Number as a Parameter

profiles at all radial and axial positions. To avoid biasing the results because of the experimental error in CMAX, the computation was carried out using the least squares analysis[49] with CMAX as the fitting parameter.

Typical results are shown in Figure 37 to 39. The numerical values of the ordinates in Figures 37 to 39 are actually the droplet impaction count data. They are, however, proportional to the concentration and are labeled as such on the graphs. The units are arbitrary since an absolute determination of concentration was not made. The circles and squares represent data from the two sides of the probe traverse. For each case, the first curve shown is the source distribution S(r), and those following it are the concentration distributions (data and computations) at positions downstream from the source plane. Although the asymmetries in the concentration profiles discussed previously are observed, the data generally agrees with the theoretical prediction within $\pm$20%.

Figure 39(c) shows the fit of the data to the diffusion model prediction for the case where d = 80μ, Re = 100,000 and z = 19 ft. This case is discussed in a previous section in reference to the large scatter in the particle diffusivity data. The diffusivity data for this set of conditions were discarded since it was suspected that a flow disturbance existed at z = 19 ft. The disturbance was probably caused by a missing plug in the tube wall, resulting in a flow of air into the tube at the site of the measurement.

In general, the diffusion model predicts the droplet concentration distributions to within $\pm$20%.

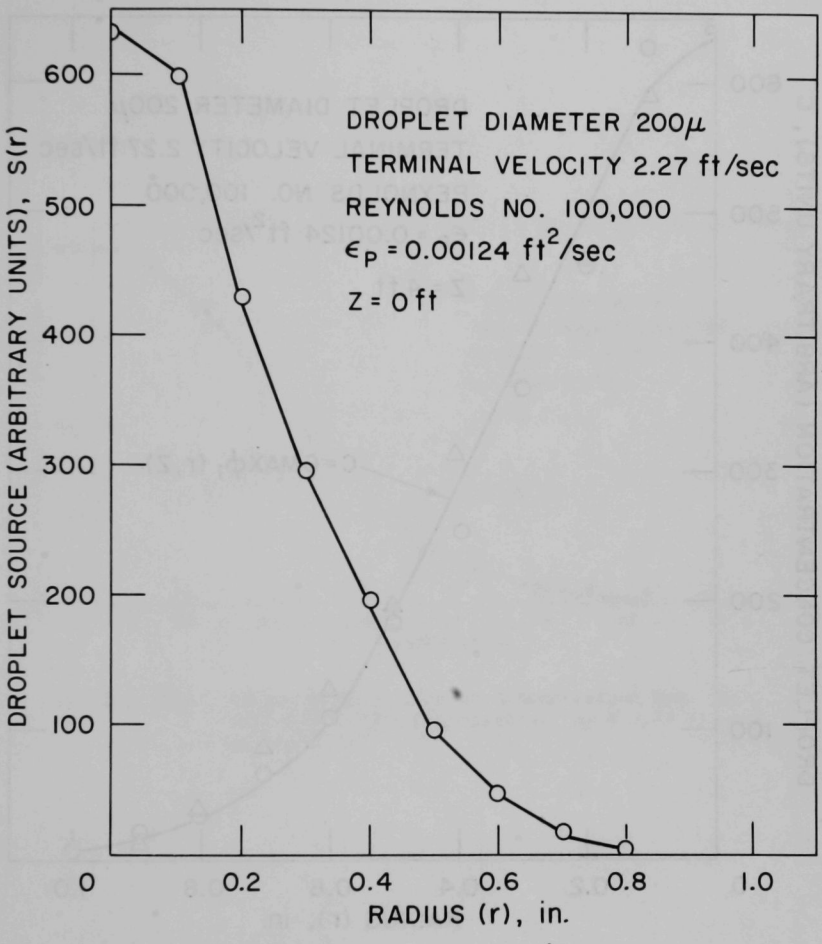

Fig. 37a. Comparisons of Droplet Concentration Data with Diffusion Model Calculation: u_t = 2.27 ft/sec, Re = 100,000

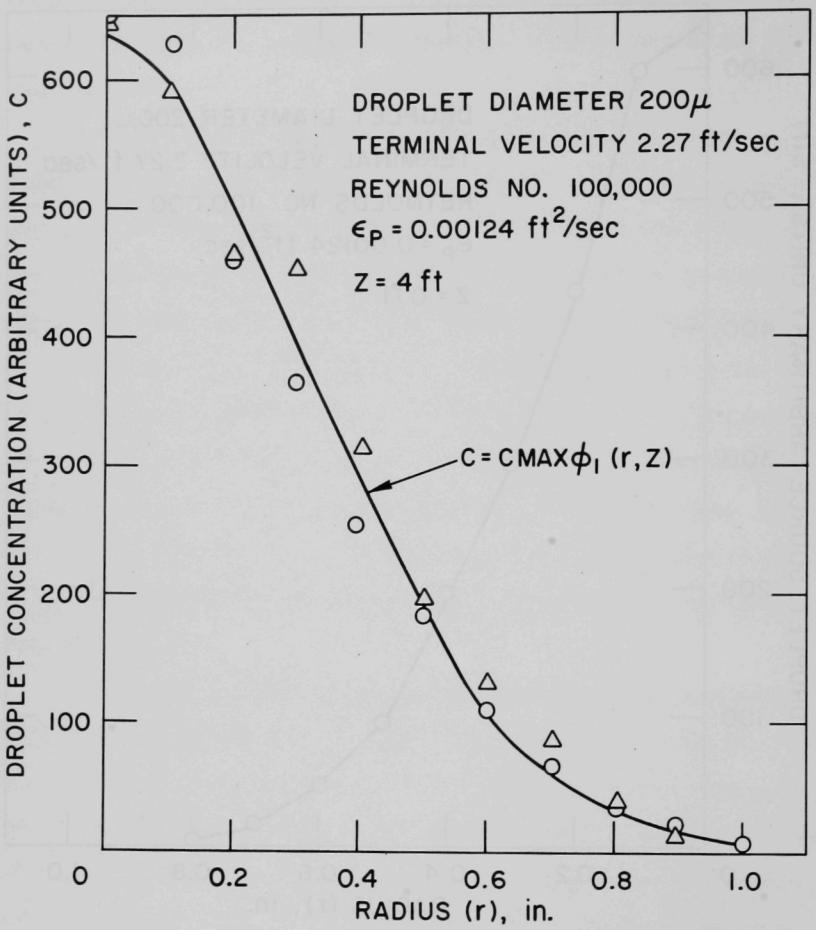

Fig. 37b. Comparisons of Droplet Concentration Data with Diffusion Model Calculation: u_t = 2.27 ft/sec, Re = 100,000

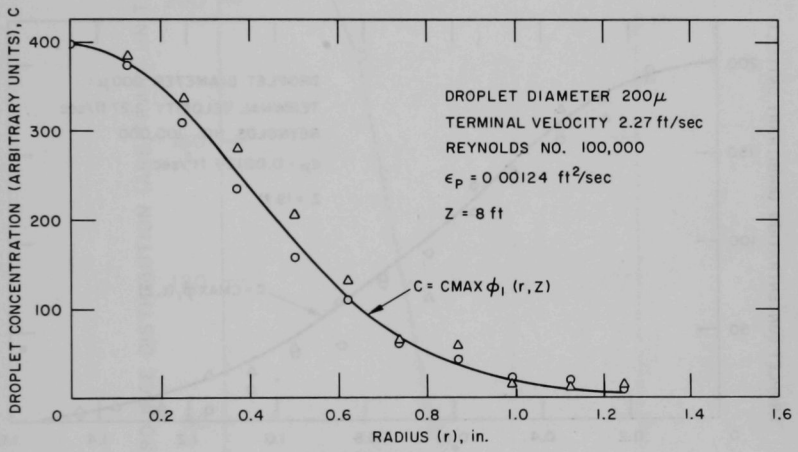

Fig. 37c. Comparisons of Droplet Concentration Data with Diffusion Model Calculation: u_t = 2.27 ft/sec, Re = 100,000

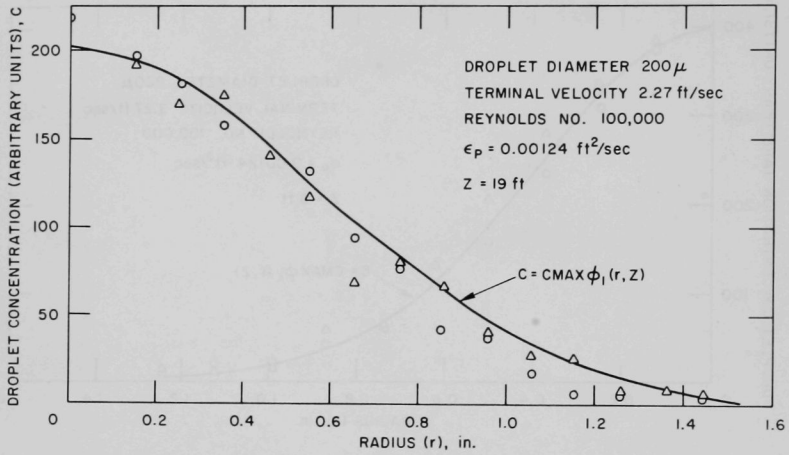

Fig. 37d. Comparisons of Droplet Concentration Data with Diffusion Model Calculation: u_t = 2.27 ft/sec, Re = 100,000

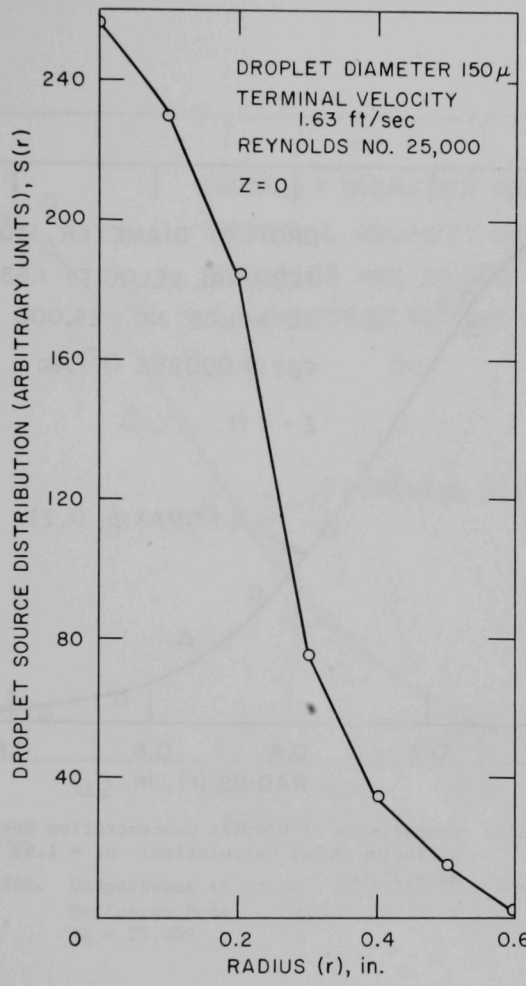

Fig. 38a. Comparisons of Droplet Concentration Data with Diffusion Model Calculation: u_t = 1.63 ft/sec, Re = 25,000

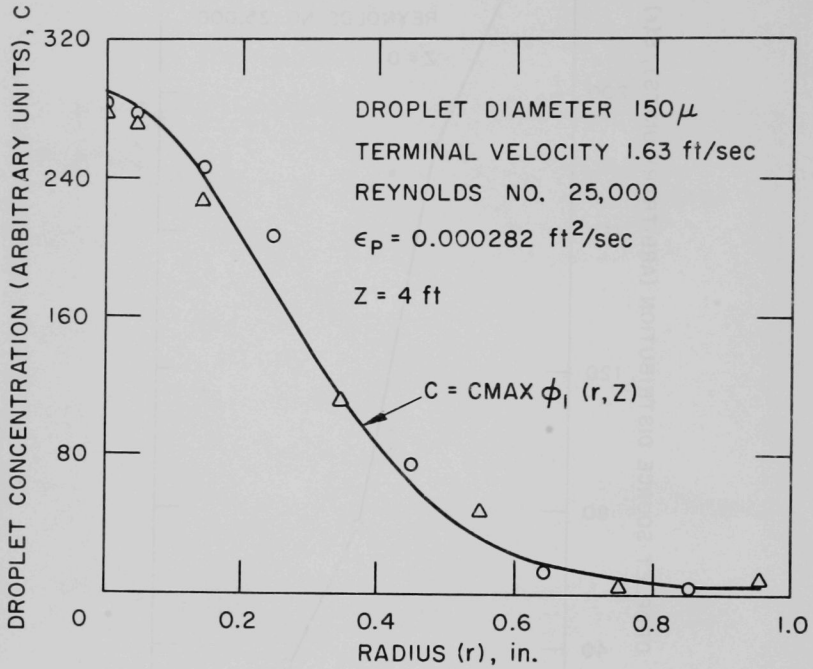

Fig. 38b. Comparisons of Droplet Concentration Data with Diffusion Model Calculation: u_t = 1.63 ft/sec, Re = 25,000

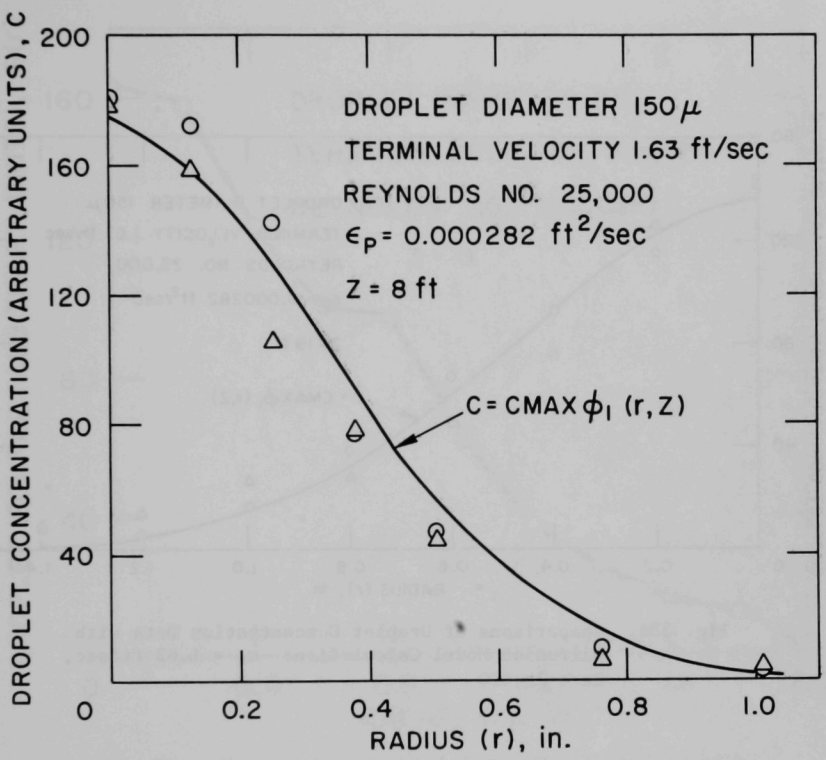

Fig. 38c. Comparisons of Droplet Concentration Data with Diffusion Model Calculation: u_t = 1.63 ft/sec, Re = 25,000

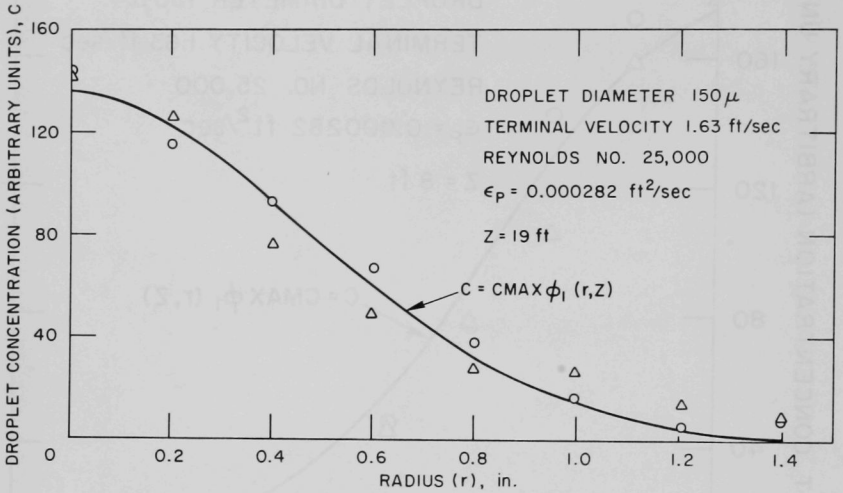

Fig. 38d. Comparisons of Droplet Concentration Data with Diffusion Model Calculation: u_t = 1.63 ft/sec, Re = 25,000

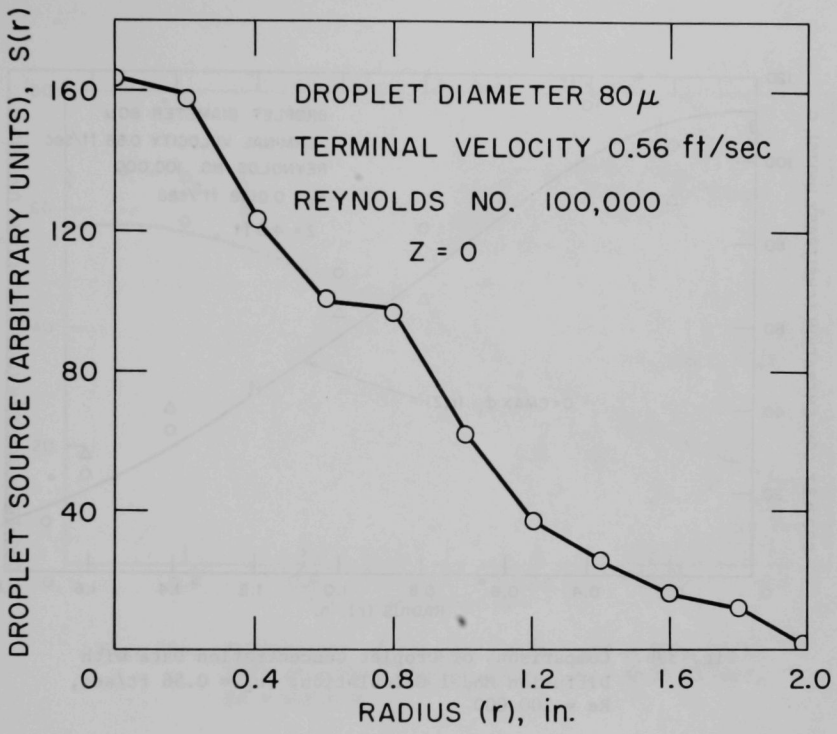

Fig. 39a. Comparisons of Droplet Concentration Data with Diffusion Model Calculation: u_t = 0.56 ft/sec, Re = 100,000

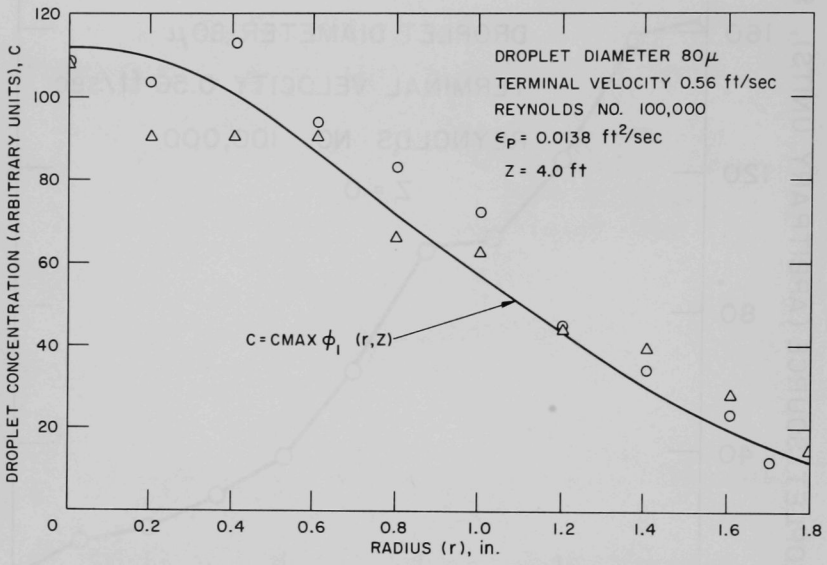

Fig. 39b. Comparisons of Droplet Concentration Data with Diffusion Model Calculation: u_t = 0.56 ft/sec, Re = 100,000

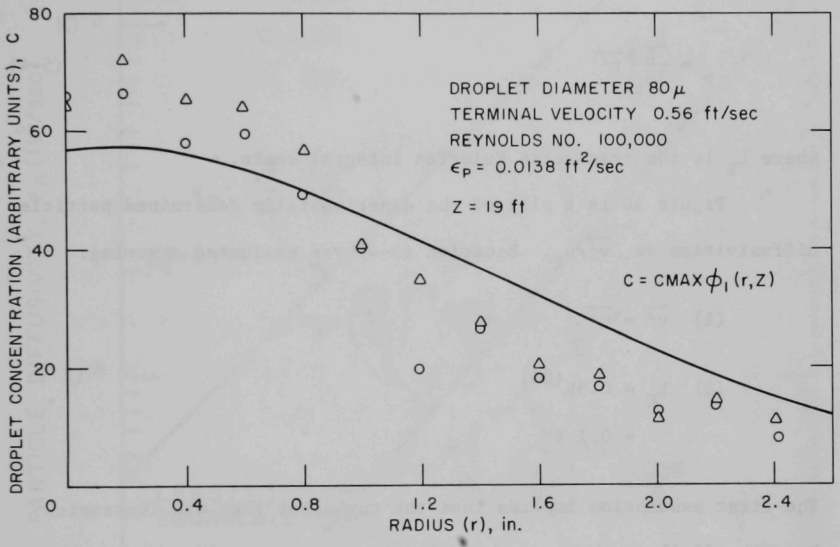

Fig. 39c. Comparisons of Droplet Concentration Data with Diffusion Model Calculation: u_t = 0.56 ft/sec, Re = 100,000

5.2.5 Comparison of Diffusivity Data with Large Terminal Velocity Approximation

For a particle with large terminal velocity falling through turbulent eddies, it is shown in Section 3.2 that the particle diffusivity is given by

$$\varepsilon_p = \frac{L_E}{2u_t} \overline{v^2} \qquad (5\text{-}4)$$

where L_E is the transverse Eulerian integral scale.

Figure 40 is a plot of the experimentally determined particle diffusivities vs. $\overline{v^2}/u_t$. Equation (5-4) was evaluated assuming:

(1) $\overline{v^2} = \overline{u^2}$,

(2) $L_E = 0.3R^{(64)}$

$= 0.1$ ft

The first assumption implies that the turbulent flow was isotropic. Equation (5-4) is shown as the solid line in Figure 40.

The diffusivity data were fitted to the equation

$$\varepsilon_p = \left(\frac{\overline{v^2}}{u_t}\right)^A \frac{B}{2}, \qquad (5\text{-}5)$$

where A and B are the fitting parameters. According to Equation (5-4), the results of the least squares analysis should be that A = 1 and B = L_E = 0.1 ft.

The results of the least squares analysis are shown in Figure 40. Curve (1) was obtained from a least squares analysis which included all the data points shown on the plot. Curve (2) was obtained by excluding

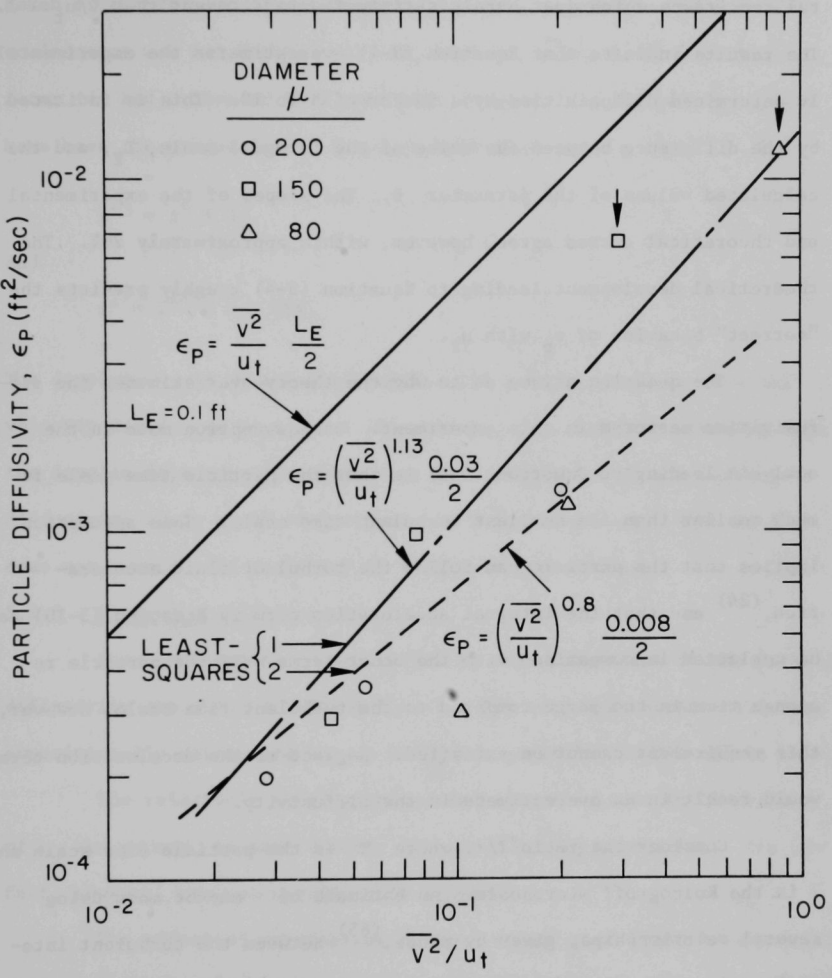

Fig. 40. Particle Diffusivity Data Compared with Theoretical Result Based on Large Terminal Velocity Approximation

the two points shown with arrows. These two points represent experimental conditions which just barely satisfy the requirement that $v/u_t < 1$. The results indicate that Equation (5-4) overestimates the experimentally determined diffusivities by a factor of 5 to 10. This is indicated by the difference between the value of the integral scale, L_E, and the calculated values of the parameter B. The slopes of the experimental and theoretical curves agree, however, within approximately 20%. The theoretical development leading to Equation (5-4) roughly predicts the "correct" behavior of ε_p with u_t.

The question arises as to why the theory overestimates the diffusivities measured in this experiment. One assumption made in the analysis leading to Equation (5-4) is that the particle time scale is much smaller than the smallest turbulent time scale. This assumption implies that the particle can follow the turbulent fluid acceleration,[24] and that the integral acceleration term in Equation (3-10) can be neglected in comparison with the other terms. If the particle response time is too large compared to the turbulent time scale, however, this requirement cannot be satisfied. Neglect of the acceleration term would result in an overestimate in the diffusivity.

Consider the ratio T/τ, where T is the particle time scale and τ is the Kolmogroff microscale. An estimate of τ may be made using several relationships, given by Hinze,[65] between the turbulent integral scales and microscales. Assume that $L_E = 0.1$ ft and that $v/U = 0.03$. The requirement $T/\tau \ll 1$ is satisfied only for the case $d = 80\mu$ and $U = 6$ ft/sec ($Re = 25{,}000$). Unfortunately, when $d = 80\mu$ the requirement of the theory that $v/u_t \ll 1$ is not satisfied.

An additional possible explanation for the overestimate of ε_p is

the following: There was evidence of droplet coalescence in photographs taken of the droplet stream emerging from the injector. The rate of coalescence was not determined. If, however, every droplet with diameter d had coalesced with one other droplet, the net effect would have been the production of droplets with diameter d', where

$$d'^3 = d^3 + d^3,$$

and

$$d' = 2^{1/3}d = 1.26d.$$

The droplets would have had a diameter 26% greater, and the terminal velocity would have been about 50% greater, than droplets emerging from the droplet injector. The effect on the calculation of the particle diffusivity would be an overestimate by a factor of two. This still does not account for the order of magnitude discrepancy.

5.2.6 Experimental Errors

The experimental uncertainties in the measurement of the particle diffusivity are shown in Tables 1 to 3. The standard deviations in the experimentally determined values of ε_p are generally 10-25% of the mean.

The relatively large standard deviations evident in the values of ε_p are caused, to some extent, by poor counting statistics. Its effect, however, was not specifically examined.

The effect of asymmetries in the droplet flow field is apparently reflected in the discrepancy between the diffusivities calculated from droplet flux data on either side of the centerline. Differences of as much as 35-40% between the two values are observed. This leads to relatively large uncertainties in the measurements. Accuracy probably could be improved by making more detailed measurements of the flow distribu-

tions at each axial location, i.e., by making probe traverses at several azimuthal angles, and then reducing the data using the two-dimensional diffusion equation.

Since liquid droplets, rather than solid particles, were employed in this research, the effects of droplet coalescence, evaporation, and breakup on the results are considered next.

Photographs of the droplet stream just downstream of the injector revealed the possible occurrence of droplet coalescence. This problem was not considered further, since most of the data were already collected when the possibility of coalescence near the source was observed. The 25% increase in drop size and corresponding 50% increase in terminal velocity, discussed in Section 5.2.5, are probably overestimates. The effect should be considered further, however, in future studies.

The change in drop at diameter and, hence, terminal velocity, caused by evaporation may be estimated with the equation:[61]

$$-\frac{dm}{dt} = \frac{D_o}{RT_o}\ 4\pi r\ (p_i - p)\ , \qquad (5\text{-}6)$$

where

m = droplet mass

D_o = diffusion coefficient for water vapor in air

T_o = absolute temperature

R = gas constant

p_i = partial pressure of water at liquid-vapor boundary

p = partial pressure of water at $r = \infty$

r = r(t) drop radius [r_o = r(o)]

t = time .

Assume that saturated conditions exist at the interface and that the air is completely dry at $r = \infty$. Integrate Equation (5-6). The result is

$$r^2 - r_o^2 = -0.1 \times 10^{-4} t(cm^2).$$

The worst case occurred for $d = 80\mu$ and Re = 100,000. The droplet residence time in the duct was approximately 3 seconds. For this case, then,

$$\frac{\Delta r^2}{r_o^2} = -0.42,$$

and

$$\frac{\Delta r}{r_o} = -0.21.$$

The droplet diameter decreased by 21% and terminal velocity by 42% (assuming $\varepsilon_p \propto u_t^{-1}$) while the droplet traveled from the source to the flow tube exit. The values of ε_p deduced from data taken at the last axial measurement station should consequently be greater than those deduced from data taken at positions upstream. This is not observed in the data shown in Tables 1 to 3. Equation (5-6) may be used to correct the data to account for evaporation. This was not done, however, since the evaporation effect is not observed.

The above calculation was based on the droplet residence time in the flow tube. The change in droplet diameter caused by droplet evaporation is proportional to the distance from the injector. Consequently, if the measurements are confined to axial positions close to the source,

the magnitude of the change in ε_p can be reduced to about 10-20% (for z = 5-10 ft). For the case d = 80μ, Re = 100,000, and z = 8 ft, the calculation shows that ε_p is affected by about 15%. For other sets of droplet diameter and velocity, Equation (5-6) shows that evaporation caused negligible change in ε_p at the measurement stations upstream from z = 19 ft. The change in ε_p was less than 20% for all cases.

The probability of droplet breakup may be estimated by considering the balance of surface tension and aerodynamic pressure forces acting on a droplet. Lane[62] studied the breakup of water droplets, with diameters between 500 - 5000μ, in an air stream. He showed that breakup occurs if $U_r^2 d > 612$, where U_r(m/sec) is the relative velocity between air and droplet and d(mm) is the diameter. In the experiment performed here, the most likely situation for breakup occurred for d = 200μ and U_r = 30 ft/sec, where U_r is the relative velocity of a droplet as it leaves the injector. For this case, $U_r^2 d = 20$. Lane's results, assuming they are applicable to 200μ droplets, imply that droplet breakup did not occur in these experiments.

VI. CLOSURE

6.1 Problem Statement

This research was initiated to investigate the application of the Fick's law turbulent diffusion model, as applied to droplet transport in the two phase fog flow boiling regime.

The objectives of the analytical work were:

(1) To define the Fick's law turbulent diffusion model, as applied to the description of droplet transport in turbulent flow.

(2) To analyze the momentum equation for a single droplet in turbulent flow, in an attempt to obtain an expression for the particle diffusivity as a function of droplet parameters and turbulent flow characteristics.

The objectives of the experimental investigation were:

(1) To determine whether the turbulent diffusion model, with constant diffusivity, can be used to predict the droplet concentration distribution downstream from a source of droplets in the central core region of fully developed turbulent pipe flow.

(2) To measure the particle diffusivity as a function of droplet parameters and turbulent flow characteristics.

6.2 Summary and Conclusions

The literature dealing with the critical heat transfer condition in the convective boiling regimes is reviewed. Particular emphasis is placed on the fog flow boiling regime, and on proposed models of the

droplet transport process which are found in the critical heat transfer literature. The turbulent diffusion literature is reviewed. The review includes a discussion of the eddy diffusion model of turbulent transport. Past investigations concerning the transport of particulate matter in turbulent flow are discussed.

The Fick's law diffusion model of turbulent droplet transport is defined, and its implications are discussed. The model is applied to the transport of droplets in the central core region of fully developed pipe flow. For this case, the one-dimensional diffusion equation is used to describe the droplet concentration distribution downstream from an arbitrary, axially symmetric source of droplets. Two solutions to the diffusion equation are presented: The first for a point source of droplets, and the second for a plane source of droplets.

An analysis is made of the momentum equations for a single droplet moving in a turbulent fluid. The Bassett-Boussinesq-Oseen equations, and Tchen's modification of these equations, are presented. Tchen's formulation, based on the assumption that a particle is surrounded by the same fluid eddy at all times, leads to linear equations of particle motion. In this formulation, the Eulerian fluid velocity is considered independent of spatial coordinates. One implication of the linear formulation is that the particle diffusivity is equal to the fluid diffusivity, independent of particle parameters and fluid turbulence characteristics. This conclusion is valid for particles whose response times are much less than the smallest time scale of the turbulence, and whose diameters are much less than the smallest length scale of the turbulence. The reduction of the general equations of particle motion to Lumley's integral equation is discussed. The significant feature of Lumley's

formulation is that the particle is not constrained to follow a single fluid eddy during its history of motion. The Eulerian fluid velocity depends on spatial coordinates, and the equations of motion are, therefore, nonlinear.

A solution to Lumley's integral equations is obtained for the case of a particle falling with terminal velocity greater than the rms turbulent velocity. The particle diffusivity is shown to be

$$\varepsilon_p = \frac{L_E}{2u_t} \overline{v^2} \quad . \tag{6-1}$$

A flow facility was designed and constructed to provide a fully developed turbulent pipe flow of air in which to carry out the droplet transport experiments. A flow tube, 7.5 inches in diameter and 38 feet long (61 tube diameters), was designed with suitable entry and flow development sections to ensure fully developed flow at the site of the experiments. The facility was provided with a flanged section, two feet long, to allow insertion of a source of liquid droplets into the flow tube.

Mean and turbulent air velocity measurements were carried out with a constant temperature hot wire anemometer, operated at a hot-to-cold resistance ratio of 1.5. A digital data acquisition system was used to convert the instantaneous output data to digital form and to record the data on paper tape. The data were time averaged and the velocities calculated on a CDC-160A digital computer. Hot wire traverses were made 17.6, 33.6, 40.0, and 57.2 diameters from the inlet to the flow tube and at Reynolds numbers: 25,000, 50,000 and 100,000. The purpose of these measurements was to establish the state of development of the

turbulent pipe flow and to determine the mean velocity and turbulent intensity distributions.

The data indicate that the air flow was nearly fully developed 30-40 diameters from the inlet to the flow tube. Asymmetries in the flow were observed in the mean velocity and turbulent intensity distributions. The asymmetries were carried downstream to the site of the droplet measurements. The mean velocity distributions compare favorably with Laufer's[50] data. The axial intensity distributions show deviation from Laufer's data, but centerline intensities compare well with Laufer's and other data. Axial pressure drop measurements indicate that the pressure gradient was constant over the length of tube where droplet measurements were carried out.

A droplet injection device, developed elsewhere,[55,56,57] was modified to suit the requirements of this investigation. The device introduced a stream of droplets into the turbulent flow field. The injector, based on the Rayleigh instability of a cylindrical laminar liquid jet, produced a continuous stream of uniform size droplets of known diameter. The injector system, with additional modification, is capable of producing droplets in the diameter range 25 to 350 microns.

Droplet concentration measurements were made downstream from the droplet injector. A constant temperature hot wire anemometer, operated at a resistance ratio of 1.5, was employed as a droplet sensor. The anemometer produced a voltage spike each time a droplet impacted on the wire. The droplet impaction count rate was measured. The count rate is shown to be proportional to droplet number flux. Assuming a radially uniform axial droplet convective velocity, the flux is shown to be proportional to the local droplet concentration.

The droplet concentration measurements were carried out with three droplet sizes: 80μ, 150μ, and 200μ. These correspond to terminal velocities: 0.57, 1.63 and 2.27 ft/sec. Three Reynolds numbers were considered: 25,000, 50,000, and 100,000.

The concentration data reduction was carried out to determine ε_p as a function of droplet terminal velocity and mean flow Reynolds number. Least squares analyses were performed on the droplet concentration data; the data were fitted to the point and plane source solutions of the diffusion equation. For each droplet size, Reynolds number and axial measurement station, this fitting procedure yielded a value of the particle diffusivity.

No significant differences are found in the values of the particle diffusivities extracted from the least squares fits of the data to the point and plane source solutions to the diffusion equation. The source of droplets employed in these experiments can, therefore, be represented as an idealized point source, represented by a Dirac delta-function.

No systematic variation of the particle diffusivity with axial position from the source of droplets is observed. Within the accuracy of the experiments ($\pm$20-30%), therefore, the particle diffusivity is independent of axial position from the source.

The plane source solution to the diffusion equation was used, together with the measured plane source distribution, to calculate the concentration distributions downstream from the source. The diffusivity used in the calculation was taken from Figure 34. The computational results, based on a value of ε_p independent of radius and of axial position, fit the experimental concentration data generally within $\pm$20%.

The particle diffusivity data show qualitative agreement with Equation (6-1). The diffusivity decreases with terminal velocity and increases with mean flow Reynolds number. Equation (6-1) implies that $\varepsilon_p \propto 1/d^2$. Results of least squares analyses of the diffusivity data show that $\varepsilon_p \propto 1/d^n$, where $1.60 < n < 2.26$. The behavior of the particle diffusivity with particle diameter agrees with the theoretical prediction within $\pm 20\%$. The least squares results, however, show that Equation (6-1) overestimates the data by a factor of 5 to 10. The reasons for the overestimate are not clear at this time, although some speculations are made in Section 5.2.5.

A comparison of the particle diffusivity results with literature values of ε_f, the turbulent mass diffusivity, shows that the ratio $\varepsilon_p/\varepsilon_f$ is close to unity for $d = 80\mu$ and $Re = 100{,}000$. This indicates that at this Reynolds number, water droplets with diameter less than 80μ behave as particles with negligible inertia as far as turbulent mixing behavior is concerned. Additional measurements for $d < 80\mu$ are needed to substantiate this point. In addition, the ratio $\varepsilon_p/\varepsilon_f$ is found to increase with mean flow Reynolds number. This evidence is contrary to the results of other investigations appearing in the literature and is not predicted by the linear theory of particle motion.

Aside from the hot wire anemometer, three other experimental techniques for the measurement of droplet flow properties were tested. Two fiber optic light attenuation probes were developed to sense local droplet concentration. Attempts to use the first were unsuccessful because of problems with droplet deposition on the sensing faces of the fiber bundle. The second probe was constructed to allow for an air purge to clean the sensing faces of the fiber bundle of deposited drop-

lets . Although this technique was successful in clearing the liquid from the sensing faces, droplet deposition occurred too fast after the purge for the concentration measurements to be successfully made.

Successful application of the diffusion model to turbulent particle transport in practical situations, requires knowledge of the particle diffusivity as a function of terminal velocity and turbulent flow parameters. Assuming that this information is available, knowledge of the particle size distribution encountered in practice is required. This information, however, is difficult to obtain. That this data is required is shown in this work, as evidenced by the strong dependence of the diffusivity on the experimental parameters.

Application of the model to the transport of droplets in the two phase fog flow boiling regime is expected to present difficulty. Information regarding droplet size distributions in this situation is extremely difficult to obtain. Since the particle diffusivity depends on the properties of the turbulent flow, information obtained in the controlled laboratory experiment should not be expected to apply very satisfactorily to nuclear reactor flow channels, where the flow patterns are extremely complex, and about which information is difficult to obtain. In addition, the simultaneous occurrence of droplet evaporation, coalescence and breakup may be expected to further complicate the situation. In conclusion, this investigation has shown that the Fick's law diffusion model can be used to describe the turbulent diffusion mechanism, but much work remains to be done before the model can be applied to the description of the fog flow regime.

6.3 Suggestions for Future Research

The experiments described here should be extended to obtain par-

ticle diffusivity data for droplets with diameter less than those considered here ($d < 80\mu$). This information could be interpreted in a manner to determine for what range of droplet diameter the linear theory of particle motion is valid ($\varepsilon_f = \varepsilon_p$). In the course of this investigation the droplet coalescence problem could be more carefully examined. In addition, it would be of interest to obtain data on the turbulent diffusion of gases in the apparatus described here, and to compare the results with the particle diffusivity data.

The next step in the development of a model of the fog flow regime should be an investigation of the turbulent transport process for the case where droplets occupy the entire tube cross section and interact with the walls. The possibility of extending the diffusion model to include a radially dependent particle diffusivity should be considered. In addition, the boundary condition on the droplet diffusion equation for the case where droplets impact on duct walls should be investigated.

Further investigation of the relation between Lagrangian particle statistics and the Eulerian description of the turbulence is necessary to obtain further information about the validity of the large particle terminal velocity approximation to the droplet momentum equation. It is suggested that the alternate method of obtaining particle trajectory information be pursued to this end, i.e., by following the motion of a single particle through its flight history. This would yield more detailed information about the particle trajectory statistics than is possible to obtain with the technique employed here.

APPENDIX A

Statistical Description of Turbulent Flow

Turbulent flows are characterized by irregular fluid motion in time and space. It is, therefore, necessary to discuss these motions in statistical terms. The following is a brief discussion of the statistical terminology applied to the study of turbulent flow.

When the Navier-Stokes' equations are applied to turbulent flow, there appear in the resulting equations statistical quantities called correlation functions.

A spatial correlation function between velocities at positions x and $x + x'$ may be defined as follows:

$$\overline{u(x)u(x + x')} = R_x(x,x')\overline{u^2(x)},$$

where the over-bar represents a time average of the quantities beneath it. At zero separation, $x' = 0$, the velocities are "perfectly correlated" and $R_x = 1$. For large x' the velocities are uncorrelated and $R_x = 0$. If R_x is independent of x then the flow is called homogeneous in the x direction. For this case $R_x(x,x') = R_x(x')$.

The correlation function described above is one between velocities at fixed points in the flow and is called an Eulerian correlation function. Another type of function may be defined by following the motion of a fluid "lump" through the flow field. A correlation function may be defined in terms of the velocity of the "lump" at successive times along its trajectory. This is a Lagrangian correlation function.

The integral scale is a measure of the distance, or time inter-

val, over which velocities are well correlated. An Eulerian length scale may be defined by

$$\Lambda = \int_0^\infty R_x(x')dx'$$

Physically, the length scale can be considered as a characteristic dimension of the largest "eddy" present in a turbulent flow.

Many other correlation functions and scales of turbulence may be defined and are meaningful in the analysis of turbulent flow. The above discussion, however, should suffice for the purpose of familiarizing the reader with the terminology that is used in the body of this work. The reader is referred to Reference 23 for further elaboration.

ACKNOWLEDGEMENTS

The author wishes to express his gratitude to the many people who gave their aid and encouragement during the course of this investigation. Special thanks are extended to Mr. Ralph P. Stein, who suggested the work and gave constructive criticisms throughout the investigation. Thanks are also extended to Dr. Alan M. Jacobs, for his interest and suggestions; to Dr. John Lumley, for his aid in the analytical portion of this study; to Mr. Matthew Featherstone, who aided in the construction and operation of the experimental apparatus; and to Mr. Albert Moessner, who fabricated several of the components.

This investigation was supported by the joint fellowship program of Associated Midwest Universities and Argonne National Laboratory. The research was carried out under the auspices of the United States Atomic Energy Commission, Division of Reactor Development and Technology, Engineering Development Branch.

REFERENCES

1. Stein, R. P., and Lottes, P. A., "Boiling Burnout for Reactor Design," Reactor Technology, Selected Reviews - 1964 (ed.) L. E. Link, TID-8540, pp. 131-176.

2. Stein, R. P., "Fog-Flow Models," Proc. 2nd Joint USAEC Euratom Two-Phase Flow Meeting, Germantown, Md., CONF 640507 (1964), pp. 367-385.

3. Tippets, F. E., "Analysis of Critical Heat-Flux Condition in High Pressure Boiling Water Flows," ASME Trans. Ser. C, J. Heat Transfer, 86(1), 23-28 (Feb 1964).

4. Isbin, H. S., Fauske, H., Vanderwater, R., and Singh, R., "A Model for Correlating Two-Phase, Steam-Water, Burnout Heat-Transfer Fluxes," ASME Trans., Ser. C, J. Heat Transfer, 83(2), 149-157 (May 1961).

5. Grace, T. M., "The Mechanism of Burnout in Initially Subcooled Forced Convective Systems," Ph.D. Thesis, University of Minnesota (1964).

6. Goldmann, K., Firstenberg, H., and Lombardi, C., "Burnout in Turbulent Flow - A Droplet Diffusion Model," ASME Trans., Ser. C, Heat Transfer, 83(2), 158-162 (May 1961).

7. Randles, J., "A Theory of Burnout in Heated Channels at Low Mass Velocities," AEEW-R279 (1963).

8. Vanderwater, R. G., "An Analysis of Burnout in Two-Phase, Liquid-Vapor Flow," Ph.D. Thesis, University of Minnesota (1956).

9. Stein, R. P., et al., "Investigation of Wet Steam as a Reactor Coolant (Can-2)," United Nuclear Corp., UNC-5008-I (Aug 1962), Vol. I: Behavior of a Fog Flow as a Coolant. Final Report.

10. Taylor, G. I., "Diffusion by Continuous Movements," Proc. Lond. Math. Soc., 20, 196-212 (1922).

11. Hinze, J. O., "Turbulence", McGraw-Hill, New York (1959), p. 20.

12. Einstein, A., "Investigations on the Theory of Brownian Movement," Dover Publications, New York (1956).

13. Dryden, H., "Turbulence and Diffusion," Ind. Eng. Chem. 31(4), 416-425 (1939).

14. Batchelor, G. F., "Diffusion in a Field of Homogeneous Turbulence, I: Eulerian Analysis," Aust. J. Sci. Res. A. 2, 437-450 (1949).

15. Hewitt, G. F., and Lacey, P. M. C., "The Breakdown of the Liquid Film in Annular Two-Phase Flow," AERE-R4303 (1963).

REFERENCES (Contd.)

16. Taylor, G. I., "Statistical Theory of Turbulence, IV: Diffusion in a Turbulent Air Stream," Proc. Roy. Soc. A., 151, 465-478 (1935).

17. Schubauer, G. B., "A Turbulence Indicator Utilizing the Diffusion of Heat," NACA Technical Report No. 524 (1935).

18. Baldwin, L. V., and Walsh, T. J., "Turbulent Diffusion in the Core of Fully Developed Pipe Flow," AIChE J. 7(1), 53-61 (Mar 1960).

19. Flint, D. L., Kada, H., and Hanratty, T. J., "Point Source Turbulent Diffusion in a Pipe," AIChE, J. 6(2), 325-331 (1960).

20. Bird, R. B., Stewart, W. E., and Lightfoot, E. N., "Transport Phenomena," John Wiley and Sons, New York (1960).

21. Basset, A. B., "A Treatise on Hydrodynamics," Vol. 2, Dover Publications, New York (1961).

22. Landau, L. D., and Lifshitz, E. M., "Fluid Mechanics," Addison Wesley Publishing Co., Reading, Mass. (1959), p. 85.

23. Hinze, J. O., "Turbulence," McGraw Hill, New York (1959), Chap. 5.

24. Lumley, J. L., "Some Problems Connected with the Motion of Small Particles in a Turbulent Fluid," Ph.D. Thesis, Johns Hopkins University (1957).

25. Friedlander, S. K., "Behavior of Suspended Particles in a Turbulent Fluid," AIChE, J. 3(3), 381-385 (Sept 1957).

26. Soo, S. L., "Fully Developed Turbulent Pipe Flow of a Gas-Solid Suspension," Ind. Eng. Chem. Fund. 1(1), 33-37 (Feb 1962).

27. Csanady, G. T., "Turbulent Diffusion in a Stratified Fluid," J. Atmos. Sci. 21(4), 439-447 (1964).

28. Hjelmfelt, A. T., and Mockros, L. F., "Motion of Discrete Particles in a Turbulent Fluid," Appl. Sci. Res. 16, 149-161 (1966).

29. Peskin, R. L., "The Diffusivity of Small Suspended Particles in Turbulent Fluids," National Mtg. AIChE, Baltimore (1962).

30. Soo, S. L., Ihrig, H. K., and ElKouh, A. W., "Experimental Determination of Statistical Properties of Two-Phase Turublent Motion," ASME Trans., Ser. D, J. Basic Eng., 82(3), 609-621 (Sept 1960).

31. Jones, B. G., "An Experimental Study of the Motion of Small Particles in a Turbulent Fluid Field Using Digital Techniques for Statistical Data Processing," Ph.D. Thesis, University of Illinois (1966).

32. Frenzen, P., "A Laboratory Investigation of the Lagrangian Autocorrelation Function in a Stratified Fluid," ANL-6794 (Nov 1963).

REFERENCES (Contd.)

33. Soo, S. L., "Fluid Dynamics of Multiphase Systems," Blaisdell Publishing Co., Waltham, Mass. (1967).

34. Soo, S. L., and Regalbuto, J. A., "Concentration Distribution in Two-Phase Pipe Flow," Can. J. Ch.E., 38, 160-166 (Oct. 1960).

35. Soo, S. L., et al., "Concentration and Mass Flow Distributions in a Gas-Solid Suspension," Ind. Eng. Chem. Fund. 3(2), 98-106 (May 1964).

36. Soo, S. L., "Effect of Electrification on the Dynamics of a Particulate System," Ind. Eng. Chem. Fund, 3(1), 75-80 (Feb 1964).

37. Soo, S. L. and Peskin, R. L., "Statistical Distribution of Solid Phase in Two-Phase Turbulent Motion," Project Squid Technical Report No. PR-80-R (1958).

38. Wakstein, C., "The Motion of Small Particles Suspended in Turbulent Air Flow in a Vertical Pipe," Ph.D. Thesis, Queen Mary College (1966).

39. Alexander, L. G., and Coldren, C. L., "Droplet Transfer from Suspending Air to Duct Walls," Ind. Eng. Chem., 43(6), 1325-1331 (1951).

40. Longwell, J. P., and Weiss, M. A., "Mixing and Distribution of Liquids in High Velocity Air Streams," Ind. Eng. Chem., 45(3), 667-677 (Mar 1953).

41. Goldschmidt, V., and Eskenazi, S., "Two-Phase Turbulent Flow in a Plane Jet," ASME Trans., Ser. E, J. Appl. Mech., 33(4), 735-757 (Dec 1966).

42. Goldschmidt, V. W., "Measurement of Aerosol Concentrations with a Hot-Wire Anemometer," J. Colloid Sci., 20(6), 617-34 (1965).

43. Kada, H., and Hanratty, R. J., "Effects of Solids on Turbulence in a Fluid," AIChE J., 6(4), 624-630 (1960).

44. Hinze, J. O., "Turbulence," McGraw-Hill, New York (1959), p. 536.

45. Carslaw, H. S., and Jaeger, J. C., "Conduction of Heat in Solids," 2nd Ed., Oxford Clarendon Press (1959), p. 266.

46. Corrsin, S., and Lumley, J. L., "On the Equation of Motion for a Particle in a Turbulent Fluid," Appl. Sci. Res., Sec. A, 6, 114-116 (1956).

47. Lumley, J. L., Private Communication (Aug 1969).

48. Fuchs, N. A., "The Mechanics of Aerosols," Pergamon Press, New York (1964).

49. Gabriel, M., "Special-purpose Language for Least-squares Fits," ANL-7495 (Sept 1968).

REFERENCES (Contd.)

50. Laufer, J., "The Structure of Turbulence in Fully Developed Pipe Flow," NACA Report No. 1174 (1954).

51. Coantic, M., "Contribution to the Study of the Structure of Turbulence in a Circular Duct," Ph.D. Thesis, University of Marseille (1966).

52. Resch, F., "Studies on Hot-Wire and Hot-Film Under Water," French Atomic Energy Commission, CEA-R-3510 (1968), p. 41.

53. Fuchs, N. A., and Sutugin, A. G., "Generation and Use of Monodisperse Aerosols," Aerosol Science, (ed.) Davies, C. N., Academic Press, New York (1966), Chap. 1.

54. Lamb, Sir Horace, "Hydrodynamics," 6th Ed., Dover Publications, New York (1945), p. 471.

55. Lindbald, N. R., and Schneider, J. M., "Method of Producing and Measuring Charged Single Droplets," Review of Scientific Instruments, 38(3), 325-327 (Mar 1967).

56. Schneider, J. M., and Hendricks, C. D., "Source of Uniform-Sized Liquid Droplets," Rev. Sci. Instrum., 35(10), 1349-1350 (Oct 1964).

57. Schneider, J. M., et al., "Stability of an Electrified Liquid Jet," J. Appl. Phys., 38(5), 2599-2605 (May 1967).

58. Perskin, R. L., and Dwyer, H. A., "A Study of the Mean Flow Characteristics of Gas Solid Suspensions," Rutgers University, Mechanical Engineering Department, Technical Report No. 101-ME-F (1964).

59. Schraub, F. A., "Isokinetic Sampling Probe Technique - Applied to Two-Component, Two-Phase Flow," General Electric Company, GEAP-5287 (Nov 1966).

60. Shires, G. L., and Riley, P. J., "The Measurement of Radial Voidage Distribution in Two-Phase Flow by Isokinetic Sampling," AEEW-M650 (1966).

61. Duffie, J. A., and Marshall, W. R., "Factors Influencing the Properties of Spray-Dried Materials," Chem. Eng. Prog., 49(9), 480-486 (1953).

62. Lane, W. R., "Shatter of Drops by High Velocity Air Streams," Ind. Eng. Chem., 43(6), 1312-1317 (1951).

63. Schlichting, H., "Boundary Layer Theory," 4th Ed., McGraw-Hill, New York (1960), p. 488.

64. Hinze, J. O., "Turbulence," McGraw-Hill, New York (1960), p. 185.

65. Ibid, p. 533.

B